Section 3 Optics and Devices

Chapter 1. Optics and Quantum Electronics

Academic and Research Staff

Professor Hermann A. Haus, Professor Erich P. Ippen, Professor James G. Fujimoto, Professor Peter L. Hagelstein, Professor Louis D. Smullin, Dr. Santanu Basu Dr. Brett E. Bouma, Dr. Joseph A. Izatt

Visiting Scientists and Research Affiliates

Dr. Lucio H. Acioli, Dr. Artur D. Gouveia-Neto, Dr. Franz X. Kärtner, Dr. Charles P. Lin, Dr. Jeróme M. Paye, Dr. Matasaka Shirasaki, Yuzo Hirayama

Graduate Students

Laura E. Adams, Ziad J. Azzam, Keren Bergman, Igor P. Bilinsky, Luc Boivin, Stephen A. Boppart, Jeffrey K. Bounds, Jerry C. Chen, Tak K. Cheng, Jay N. Damask, Ali M. Darwish, Christopher R. Doerr, David J. Dougherty, Siegfried B. Fleischer, Marc Fleury, James G. Goodberlet, Katherine L. Hall, Michael R. Hee, David Huang, Charles T. Hultgren, Sumanth Kaushik, Farzana I. Khatri, Gadi Lenz, Ilya Lyubomirsky, John D. Moores, Martin H. Muendel, Lynn E. Nelson, Malini Ramaswamy, Timothy A. Savas, Chi-Kuang Sun, Kohichi R. Tamura, Guillermo J. Tearney, Morrison Ulman, William Wong

Undergraduate Students

Fernando A. Broner, Darlene J. Ford, Mohammed J. Khan, Charles Yu

Technical and Support Staff

Mary C. Aldridge, Donna L. Gale, Cynthia Y. Kopf, Deborah S. Manning

1.1 Additive Pulse Modelocking

Sponsors

Joint Services Electronics Program
Contract DAAL03-92-C-0001
U.S. Air Force - Office of Scientific Research
Contract F49620-91-C-0091

Project Staff

Professor James G. Fujimoto, Professor Hermann A. Haus, Professor Erich P. Ippen, Dr. Jeróme M. Paye, Farzana I. Khatri, Gadi Lenz, John D. Moores, Lynn E. Nelson

Additive pulse modelocking (APM) is a technique of modelocking that simulates fast saturable absorber action by interferometrically transforming phase modulation caused by the Kerr effect into amplitude modulation. In its first realization with coupled cavities, where the gain was supplied by an F-center crystal, this technique was called the "soliton laser." When it was found that the fiber in the auxiliary resonator providing the phase modulation did not have to possess negative dispersion, we discovered the principle of APM.

The analytic theory of APM[1] has been developed under the assumption that a pulse experiences only small changes per pass through the laser system due to each of the phenomena participating in the pulse shaping process. This assumption covers a wide range of operating regimes, since large changes per pass tend to lead to undesirable spectral characteristics of the pulse and/or to pulse instability. Yet, there are at least two conditions under which the change per pass can be large without attendant pulse deterioration:

1. The case of large positive and negative linear dispersion in the resonator, the pulse changing in width and height due to the dispersion, the net change in one roundtrip remaining small.
2. The other condition may occur in coupled cavity systems, with large pulse changes in the nonlinear "auxilary" resonator, yet small changes in the pulse in the main resonator, due to the fact that the pulse in the auxiliary

[1] H.A. Haus, J.G. Fujimoto, and E.P. Ippen, "Structures for Additive Pulse Mode Locking," *J. Opt. Soc. Am. B* 8(10): 2068-2076 (1991).

resonator is of relatively small energy compared with the pulse in the main resonator.

Condition (1) is realized in some fiber lasers and is described in section 1.2. An analytic theory has been developed for this case which agrees with the experimental observations.[2] Contrary to the usual sech-like shape of the pulses observed in most passively modelocked systems, the pulses are approximately gaussian, a fact verified experimentally.

Recent experiments[3] showed a very stable performance with large phase shifts and large spectral broadening of the pulse in the auxiliary resonator. The spectrum of the pulse in the main resonator is quite clean and transform limited. This is condition (2) described above. We have developed an analytic theory for this "overdriven case" coupled with computer simulations of this mode of operation.[4] This approach is made possible by the recognition that the greatly broadened spectrum of the pulse fed back from the auxiliary resonator is filtered out by the regenerative gain of the main resonator. This makes possible an approximate analytic treatment of the action of the Kerr medium (fiber). Because the system performs particularly well in this regime, an understanding of its operation helps us apply the principle to other coupled cavity systems.

1.2 Fiber Ring Laser

Sponsors

Charles S. Draper Laboratories
Contract DL-H-441692
Joint Services Electronics Program
Contract DAAL03-92-C-0001
U.S. Air Force - Office of Scientific Research
Contract F49620-91-C-0091

Project Staff

Professor Hermann A. Haus, Professor Erich P. Ippen, Christopher R. Doerr, Lynn E. Nelson, Kohichi R. Tamura

Significant progress has been made in the modelocking of fiber ring lasers. Last year pulses 452 fs long were reported. These pulses were passively modelocked using the polarization-APM principle, the interference between two polarizations causing the phase-to-amplitude conversion. This past year, graduate student Kohichi Tamura was able to generate 75 fs pulses from a fiber ring laser using a new Stretched Pulse APM principle. This new method is important for the simple reason that erbium doped fiber lasers delivering reasonable average power with short pulses have a Kerr effect that is too large. The active fiber cannot be made short (< 1.5m). The mode diameter is small throughout the entire length of the resonator. When the nonlinear phase shift in the laser resonator approaches 2π, the pulses tend to become unstable. This prevents the generation of ultrashort pulses of reasonable energies, unless ways are found to reduce the nonlinearity. The Stretched Pulse APM works with pulses that "breathe" as they circulate through the ring, remaining short only within two small sections of the overall length of the ring. The fiber ring is composed of two pieces of fiber of opposite dispersion. The gain section of erbium doped fiber is positively dispersive, the passive section closing the ring is negatively dispersive. The two dispersions approximately cancel. The pulse can expand to as much as 20 times its shortest width. By tapping off the pulse through a coupler and fiber of appropriate length, the width of the output pulse can be made to be equal to the minimum width. The Stretched Pulse principle could be applied to any laser in which the Kerr nonlinearity is excessive.

Harmonic modelocking of all-fiber lasers is essential if one aims at GHz repetition rates, since the fundamental repetition rate of a fiber laser is in the 40-100 MHz regime. Because the relaxation time of the gain medium (Er or Nd) is long compared with 1 ns, the gain medium does not stabilize the pulse energies of a harmonically modelocked fiber laser. At AT&T Bell Laboratories, harmonic modelocking was achieved using a Fabry-Perot resonator internal to the fiber ring,[5] so that each pulse seeded

---

[2] K. Tamura, E.P. Ippen, and H.A. Haus, "Theory of Ultrashort Pulse from All-fiber Ring Laser," submitted to *J. Opt. Soc. Am. B.*

[3] G. Lenz, J. Paye, F.I. Khatri, J.D. Moores, H.A. Haus, and E.P. Ippen, "Recent Developments in Additive Pulse Modelocking of Solid State Lasers," paper UOE/SSL1.4, IEEE Lasers and Electro-Optics Society 1993 Annual Meeting, San Jose, California, November 15-18, 1993.

[4] F.I. Khatri, G. Lenz, J.D. Moores, H.A. Haus, and E.P. Ippen, "Extension of Coupled-Cavity Additive Pulse Mode-Locked Laser Theory," submitted to *Opt. Commun.*

[5] G.T. Harvey and L.F. Mollenauer, "Harmonically Mode-locked Fiber Ring Laser with an Internal Fabry-Perot Stabilizer for Soliton Transmission," *Opt. Lett.* 18(2): 107 (1993).

its successor. The side-coupled resonator used at NTT accomplished the same purpose.[6] Both schemes need stabilization of the optical lengths of the two resonators involved. Graduate student Christopher Doerr achieved harmonic modelocking at 1 GHz by reversing Additive Pulse Modelocking into Additive Pulse Limiting. He simply changed the polarization transformers in the fiber ring from a configuration that provided reduced loss for increasing intensity to one that provided increased loss for increasing intensity. His system is self-stabilized.[7]

We have begun work on thulium doped fiber lasers emitting in the 1.9 μm regime. Thulium is eye-safe, has a much wider bandwidth than erbium, and a very smooth bell-shaped gain curve. APM of thulium fiber lasers will lead to pulses much shorter than those obtained with erbium. Preliminary studies on cw Fabry-Perot type thulium doped lasers showed pump induced "darkening" of the fiber that fully disappears after the pump is turned off. The process is well understood, not requiring further investigation, since the presence of lasing reduces the effect and permits pumping at a level which produces satisfactory levels of gain.

1.3 Long Distance Fiber Communications

Sponsors

MIT Lincoln Laboratory
National Science Foundation
Grant ECS 90-12787

Project Staff

Professor Hermann A. Haus, Christopher R. Doerr, Farzana I. Khatri, John D. Moores, William Wong

We have extended our simulation studies to explore high bit-rate TDM on optical fibers. Repeaterless terrestrial fiber communications operate under different constraints from those of transoceanic fiber communications. Also, the millions of miles of fiber already laid with zero dispersion at 1.3 micron wavelength require new methods of upgrading to higher bit-rates and 1.5 micron operation, since erbium amplifiers are superior to any other fiber communications amplifier. Solitons are not likely to play a role in the upgraded existing fiber network, but they do offer interesting possibilities for properly chosen fiber dispersion. We have run extensive analytic studies and computer simulations to study the effect of Raman noise, Raman self-frequency shift, soliton interaction and the Gordon-Haus effect to explore limits of achievable performance.[8]

Another important aspect of long distance propagation is optical storage. High bitrates can be stored in a fiber ring if one can maintain the zeros and ones injected into the ring indefinitely. We have developed the theory for one of these storage rings. Remarkably, Christopher Doerr in his experiments on harmonic modelocking, demonstrated the possibility of storing a random sequence of zeros and ones indefinitely by switching his harmonically modelocked fiber ring from the APL state into the APM state. Under these conditions, he was able to show that random sequences of zeros and ones can maintain themselves forever, consistent with theoretical predictions.

1.4 Squeezing

Sponsors

Charles S. Draper Laboratories
Contract DL-H-441692
Fujitsu Laboratories
U.S. Navy - Office of Naval Research
Grant N00014-92-J-1302

Project Staff

Professor Hermann A. Haus, Professor Erich P. Ippen, Keren Bergman, Luc Boivin, Jeffrey K. Bounds, Christopher R. Doerr, David J. Dougherty, Ilya Lyubomirsky, Dr. Matasaka Shirasaki, Dr. Franz X. Kärtner

The MIT effort in squeezing concentrates on the pulse excited Sagnac fiber loop reflector first proposed in 1989.[9] This scheme has the advantage of

---

6 E. Yoshida, Y. Kimura, and M. Nakazawa, "Laser Diode-pumped femto second Erbium-doped Fiber Laser with a Sub-ring Cavity for Repetition Rate Control," *Appl. Phys. Lett.* 60(8): 932 (1992).

7 C.R. Doerr, H.A. Haus, E.P. Ippen, M. Shirasaki, and K. Tamura, "Additive-pulse Limiting," *Opt. Lett.* 19(1): 31-33 (1994).

8 L. Boivin, F.X. Kärtner, and H.A. Haus, "Integrable Quantum Theory of Self-phase Modulation with Finite Response Time," *Phys. Rev. Lett.*, forthcoming; J.K. Bounds and H.A. Haus, "Quantum Noise of Raman Amplification," *J. European Opt. Soc.*, forthcoming; F.X. Kärtner, D. Dougherty, H.A. Haus, and E.P. Ippen, "Raman Noise and Soliton Squeezing," *J. Opt. Soc. Am. B*, forthcoming.

9 M. Shirasaki, H.A. Haus, and D.L. Wong, "Quantum Theory of the Nonlinear Interferometer," *J. Opt. Soc. Am. B* 6(1): 82-88 (1989).

reusing the pump as the local oscillator. The first results on squeezing[10] were achieved in a fiber with exceptionally low noise caused by Guided Acoustic Wave Brillouin Scattering (GAWBS); i.e., index fluctuations caused by thermally excited acoustic waves which change the phase of the wave propagating through the fiber. For some very narrowly defined fiber parameters, it is possible to distribute the acoustic resonances so that they do not convolve into the (low-) frequency range of the measurement window (40-90 kHz) for pulses of 100 MHz repetition rate (the rate generally produced by modelocked laser sources). The fiber used met these exceptional conditions. Since these conditions are not easily met, it is important to develop techniques that suppress the GAWBS noise. The GAWBS spectrum "rolls off" before it reaches 1 GHz. Thus, if the pulse repetition rate is 1 GHz or higher, the convolution of the GAWBS noise into the low frequency measurement window can be avoided entirely.

Graduate student Keren Bergman demonstrated the suppression of Guided Acoustic Wave Brillouin Scattering (GAWBS) in her squeezing experiments in fiber Sagnac rings by developing a low noise Nd:YLF modelocked laser source modelocked at 1 GHz. Ms. Bergman was able to obtain noise levels 5.1 dB below shot noise. The power of this method is that it can be used in any pulsed system subject to GAWBS, as long as the detection window is limited to low frequencies.[11]

Careful investigation of the parameters of the system has demonstrated that the amount of shot noise reduction is consistent with the system parameters. In fact, the peak of the gaussian pulse experiences 13 dB of squeezing, but due to the averaging of the squeezing upon detection, and the imperfect quantum efficiency of the detector, the shot noise reduction is limited to 5.1 dB. Theoretical studies have shown that with pulse preshaping[12] the shot noise reduction can be improved.

We have carried out a careful investigation of the Raman noise effect on squeezing. Raman noise is somewhat analogous to GAWBS, except for the fact that the index fluctuations are induced by optical phonons rather than acoustic ones. Thus, it is a broad-band noise that does permit reduction or elimination by the schemes proven successful in the case of GAWBS. Previous investigators have concluded[13] that the noise does not affect squeezing appreciably at presently achieved levels (5 dB shot noise reduction) and that it is pulse-width independent. Our analysis is based on new careful experiments of the silica fiber Raman gain near zero frequency offset. One finds that the gain does not rise linearly as a function of frequency offset. The consequence is that the noise is not pulse-width independent, but rather increases with decreasing pulse-width, suggesting that for pulses shorter than 1 ps the Raman noise may become important.

Since squeezed radiation quickly degenerates through loss, it is important to use it in systems that, in principle, are loss-free for the squeezed radiation. Conventional fiber gyro designs do not have this property and hence modified designs must be used. In the search for such a modified design, Mr. Doerr and Dr. Shirasaki, a visitor from Fujitsu Laboratories, have arrived at a design which not only satisfies this criterion, but has several other unique properties that could lead to an improvement in conventional fiber gyro performance. Its advantages are:

1. Conventional fiber gyros bias the Sagnac fiber loop with a nonreciprocal phase shifter, or through modulation of the input excitation. The new design biases via a simple reciprocal wave plate.

2. The design is insensitive to "drifts" in all elements to first order.

The gyro has been built and tested, and all indications are that it will meet our expectations.

An analysis of squeezing calls for an accurate quantum theory of nonlinear optical systems. The excellent agreement between theory and our experiments suggest that the theoretical analysis of single-mode quantum processes developed by us and others is a reliable description of a class of such processes. Every measurement of an optical observable involves a nonlinear process. Hence the theory developed in connection with squeezing

---

[10] K. Bergman and H.A. Haus, "Squeezing in Fibers with Optical Pulses," *Opt. Lett.* 16(9): 663-665 (1991).

[11] K. Bergman, H.A. Haus, E.P. Ippen, and M. Shirasaki, "Squeezing in a Fiber Interferometer with a GHz Pump," *Opt. Lett.* 19: (1994).

[12] C.R. Doerr, F.I. Khatri, and M. Shirasaki, "Simulation of Pulsed Squeezing in Optical Fiber with Chromatic Dispersion," *J. Opt. Soc. Am. B* 11(1): 143-149 (1994).

[13] J.K. Bounds and H.A. Haus, "Quantum Noise of Raman Amplification," *J. European Opt. Soc.*, forthcoming.

can be applied to long-standing questions about the theory of quantum measurement. One of these questions is related to the evolution of the wave function of a system subjected to a measurement. The postulate of van Neumann concerning the "collapse of the wave function" upon a measurement can be explored in detail. The collapse is an extreme form of a measurement in which perfect accuracy is achieved. Most measurements are not of this character and must be treated differently. The quantum formalism developed for nonlinear optics enables one to characterize such more general, and more realistic, measurements.[14]

1.5 Integrated Photonic Components: The Channel Dropping Filter

Sponsors

National Center for Integrated Photonic Technology
National Science Foundation
Grant ECS 90-12787

Project Staff

Jay N. Damask, Mohammed J. Khan, Professor Hermann A. Haus, Professor Leslie A. Kolodziejski, Juan Ferrera, Vincent V. Wong, Professor Henry I. Smith

The channel-dropping filter uses a combination of side-coupled quarter-wave shifted distributed Bragg reflectors to selectively tap a single wavelength-division multiplexed (WDM) channel from a central optical bus waveguide.[15] Design studies have shown that five 10 GHz and 2 GHz channels at -20 dB crosstalk can be supported in the silica and InP semiconductor material systems, respectively. Moreover, a design modification may allow over twenty 10 GHz channels to be dropped with the aforementioned crosstalk figure.

Unlike current concepts in WDM receivers, such as the Integrated $N \times N$ Multiplexer/Router, the channel-dropping filter does not terminate the entire WDM bit stream to resolve one channel. Instead, each filter taps only one channel from the optical bus, leaving the remaining channels undisturbed and adding a new degree of design freedom for the network architect. Applications for the filters range from tapping a synchronizing or triggering bit stream to building a full WDM system to optically controlling a phased-array radar. The high-Q integrated optical resonators, the requisite technology for the channel-dropping filter, can itself be used for optical digital signal processing applications.

There are four components to the current project: (1) theory and design, (2) material development, (3) fabrication of waveguides and Bragg gratings, and (4) measurement and characterization. Theoretical tools have been developed to assist device design and to assess the fabrication tolerances that must be met to repeatably manufacture these grating-based filters.

Material development is following a dual course. The InGaAsP/InP semiconductor material system is an attractive platform because MSM detectors and other components can be directly integrated with the filters. The films are being grown in Professor Kolodziejski's GSMBE system and characterized in a number of support facilities. The silica-on-silicon system is a low-loss material system that can support a larger number of WDM channels than an equivalent semiconductor-based filter system can. The silica films are deposited by diffusion and LPCVD methods in the Integrated Circuits Laboratory at MIT.

Optical and x-ray lithography is required to pattern the waveguides and Bragg gratings, respectively. A new technique called Spatial Phase-Locked E-Beam Lithography, developed jointly between the Nanostructures Laboratory, directed by Professor Smith, and IBM, has demonstrated e-beam field-to-field stitching errors of ≤ 1nm. Only with such small stitching errors can the requisite spatially-coherent gratings be written. The first set of straight and quarter-wave shifted Bragg patterns has been written for subsequent transfer to silica-based waveguides.

Careful measurement and characterization of all devices, from straight waveguides to Bragg reflectors to optical resonators to channel-dropping filters, is necessary to compile a complete understanding of the behavior and operation of the WDM filters. Both spectral and temporal measurements are required. A collaboration with Drs. J. Donnelly and S. Chinn of MIT Lincoln Laboratory has recently been formed to further the device fabrication and optical measurement components of the research.

---

[14] F.X. Kärtner and H.A. Haus, "Quantum Nondemolition Measurements and the Collapse of Wave Function," *Phys. Rev. A*, forthcoming.

[15] H.A. Haus and Y. Lai, "Narrow-band Distributed Feedback Reflector Design," *J. Lightwave Tech.* 9(6): 754-760 (1991).

We have started to investigate realizations of the channel dropping filter other than those based on the quarter wave shifted DFB resonator (QWS-DFBR). Gain gratings offer interesting new possibilities. The theoretically predicted performances are superior to QWS-DFB resonators. One remarkable property of the gain grating system is that one single side-coupled resonator can both couple out the signal from the "bus," as well as reinject it; this should be contrasted with a QWS-DFB grating structure that requires three resonators to accomplish this same function.

1.6 Ultrafast Nonlinearities in Active Semiconductors

Sponsors

Joint Services Electronics Program
Contract DAAL03-92-C-0001
National Center for Integrated Photonic Technology
U.S. Air Force - Office of Scientific Research
Contract F49620-91-C-0091

Project Staff

Ali M. Darwish, David J. Dougherty, Katherine L. Hall, Charles T. Hultgren, Gadi Lenz, Professor Erich P. Ippen

Future high bit-rate communication systems may employ devices that contain active optical waveguides. Examples of these systems include all-optical switches, wavelength shifters, and optical amplifiers. The realization and reliable performance of such devices require knowledge of the ultrafast optical nonlinearities exhibited by these active waveguide structures. For some devices, such as optical amplifiers, highly linear behavior is essential. With other devices, such as switches and wavelength shifters, large optical nonlinearities are desirable and translate into good performance. Thus, the ability to design active waveguide structures and accurately predict their nonlinear and linear characteristics is important.

For long-haul fiber communications, InGaAsP waveguides that operate around 1.5 μm wavelength are the devices of choice. For shorter distance transmission, where pulse dispersion is not detrimental, AlGaAs waveguides operating around 0.8 μm could be used as well. We have two parallel research efforts underway for the study of both of these materials systems. Studying AlGaAs and InGaAsP waveguides together gives us the unique opportunity to compare the ultrafast behavior of devices from these two materials systems. The similar dynamics that they exhibit help to reveal fundamental processes that are common to all semiconductors.

To measure ultrafast nonlinearities in an active waveguide we employ short optical pulses in a pump-probe configuration. For InGaAsP studies around 1.5 μm, we use a color center laser that generates pulses around 150 femtoseconds in duration. The AlGaAs measurements near 0.8 μm are performed with a modelocked Ti:sapphire laser that generates pulses between 80 and 120 femtoseconds. The AlGaAs experiments employ a time-division interferometer (TDI) arrangement. The TDI is a pump-probe measurement technique that gives us the ability to measure both the gain and refractive index nonlinearities induced in a waveguide by a short optical pulse. The InGaAsP experimental setup employs a heterodyne pump-probe technique that also allows measurement of both gain and refractive index dynamics.[16] The pump-probe measurements performed with these systems on InGaAsP and AlGaAs devices have enhanced our understanding of optical nonlinearities in semiconductors on a picosecond and faster time scale.

The dominant dynamics we have observed are attributed to carrier heating, spectral hole burning, and two-photon absorption.[17] In addition, the refractive index exhibits an instantaneous response which is caused by the optical Stark effect. Below-band refractive index measurements performed in AlGaAs have allowed us to characterize the resonant response exhibited by the optical Stark effect. These below-band studies have also demonstrated that free carrier absorption is an important mechanism for carrier heating and, further, that there is a delay of about 100 femtoseconds in the onset of this carrier heating response. Other above-band measurements have shown that stimulated transitions can also give rise to carrier temperature changes. In particular, carrier cooling through stim-

---

[16] K.L. Hall. *Femtosecond Nonlinearities In InGaAsP Diode Lasers,* Ph.D. diss., Dept. of Electr. Eng. and Comput. Sci., MIT, 1993; K.L. Hall, A.M. Darwish, E.P. Ippen, U. Koren, and G. Raybon, "Femtosecond Index Nonlinearities in InGaAsP Optical Amplifiers," *Appl. Phys. Lett.* 62: 1320 (1993).

[17] C.T. Hultgren, K.L. Hall, G. Lenz, D.J. Dougherty, and E.P. Ippen, "Spectral-hole Burning and Carrier Heating Nonlinearities in Active Waveguides," *Proceedings of the O.S.A. Topical Meeting on Ultrafast Electronics and Opto-electronics,* San Francisco, California, January 1993.

ulated absorption has been observed. Other studies have revealed that chirp on the pulses can lead to artifacts in the refractive index measurements. Thus, careful control of pulse chirp is essential for making accurate index measurements.

In addition to being interesting from a fundamental standpoint, these pump-probe studies of active AlGaAs and InGaAsP waveguides are of practical interest. In the future, the index dynamics we have measured and characterized could become the basis for an all-optical switch. By studying them, we can determine ways in which these nonlinearities can be enhanced or suppressed, as desired, by proper design of the waveguide structure. In some cases, the processes may not be designed away, resulting in fundamental limitations to device performance.

1.7 Femtosecond Raman Measurements in Optical Fibers

Sponsor

Joint Services Electronics Program
Contract DAAL03-92-C-0001

Project Staff

David J. Dougherty, Professor Hermann A. Haus, Professor Erich P. Ippen, Dr. Franz X. Kärtner

The magnitude and spectral dependence of the Raman gain of silica glass were studied by a number of researchers twenty years ago.[18] The results of these investigations have subsequently been used in investigations of the effect of Raman gain on pulse compression using optical fibers, and in designing fiber Raman lasers and amplifiers. Intra-pulse Raman effects, such as recently proposed theories of noise generation in squeezing experiments using solitons and the soliton self-frequency shift, depend on the low frequency region of the gain spectrum.[19] To assist further investigation of these effects, we have made new measurements of the Raman gain spectrum from 6 cm^{-1} to 900 cm^{-1} with a novel femtosecond probing technique.

The experiment used the beams of two Ti:sapphire lasers arranged to counter-propagate through 700 meters of single mode polarization preserving fiber. The pump beam was CW with a spectral width of approximately 3 GHz and a typical average power of 20 mW. The probe laser was mode-locked and provided 100 fs pulses which were coupled into a short length of fiber to provide an 80 nm broadband probe beam. The large bandwidth of the probe spectrum enabled us to obtain the Raman gain spectrum over large Stokes and anti-Stokes detunings simultaneously. In principle, the resolution of this technique is limited only by the resolution of the spectrometer and by pump back-scatter at zero detuning.

The peak gain at 440 cm^{-1} was measured to be 1.6×10^{-11} cm/W, approximately 10 percent greater than previously measured. For applications such as Raman amplifiers or lasers which use the peak of the spectrum, the Raman gain for cross-polarized pump and Stokes beams may be taken to be zero. This is true only at large Stokes detunings. Our method has enabled us to present the first direct measurements of the cross-polarized Raman gain spectrum in glass fibers. The gain peaks at around 100 cm^{-1} and rapidly decreases for larger detunings. Below 50 cm^{-1}, however, the gain has the same shape as the co-polarized spectrum and is only a factor of 0.45 smaller. Cross-polarized gain should therefore be included in calculations of effects such as the soliton self-frequency shift which are due to the low frequency Raman modes of the glass.

In addition to characterizing the Raman gain, our experiment also uncovered a new coherent coupling mechanism between counter-propagating pulses and CW beams in fibers. The effect is observed through oscillations in the signal spectrum occuring on the anti-Stokes side of the pump wavelength. The size of the signal depends linearly on the pump power, and on the square of the probe power. For probe pulses polarized parallel to the pump, the spectral oscillations always occur on the Anti-Stokes side of the pump wavelength and move with the center wavelength reference as the pump is tuned. If the probe is present in both polarization modes of the fiber, oscillations are seen on the cross polarized component of the probe, but shifted to the wavelength which has the same group velocity as the pump light.

This behavior is explained by transient Brillouin scattering of the pump followed by coherent cross-phase modulation. Sound waves launched by the

---

[18] R.H. Stolen and E.P. Ippen, "Raman Gain in Glass Optical Waveguides," *Appl. Phys. Lett.* 22: 276 (1973).

[19] F.X. Kärtner, D.J. Dougherty, E.P. Ippen, and H.A. Haus, "Raman Noise and Soliton Squeezing," submitted to *J. Opt. Soc. Am. B.*; F.M. Mitschke and L.F. Mollenauer, "Discovery of the Soliton Self Frequency Shift," *Opt. Lett.* 11: 659 (1986).

beating of the pump and probe electric fields scatter pump light backwards into the probe direction with an intensity envelope described by the impulse response of the elastic waves of the medium. This scattered electric field then heterodynes with the probe field by means of the instantaneous Kerr nonlinearity to create an oscillating, time dependent phase shift (and thus freqeuncy shift) of the highly chirped probe pulse. Because glass has large positive dispersion at 800 nm and the scattered pump light trails the zero detuning wavelength, the oscillations appear on the anti-Stokes side. So far, they have limited our resolution of the Raman gain at detunings less than 6 cm^{-1}. However, the understanding we have obtained of such dynamic frequency modulation in chirped-probe, two-beam coupling experiments should make it possible to apply this simple technique to studies of fast nonlinearities in other waveguide devices.

1.8 Coherent Phonons in Solid-State Materials

Sponsors

Joint Services Electronics Program
Contract DAAL03-92-C-0001
U.S. Air Force - Office of Scientific Research
Contract F49620-91-C-0091

Project Staff

Tak K. Cheng, Professor Erich P. Ippen

Pulses of laser light, which are short compared to the optical phonon period, can be used to impulsively generate the coherent lattice vibrations in solid state materials. Our current interest in coherent phonons is two-fold: (1) using time-resolved femtosecond spectroscopy to further our understanding of lattice and electron dynamics, and (2) exploiting the coherent phonon phenomenon to modulate the physical characteristics of the material at THz frequencies. For semimetals and narrow-gap semiconductors, the reflectivity modulations due to coherent ion motion have been particularly large (on the order of 10 percent in some materials) and have suggested significant modulation of the material's electronic structure. In these cases, we have determined that the coherent phonon excitation is caused by a mechanism we call Displacive Excitation of Coherent Phonons (DECP).[20]

The DECP mechanism uses the pump pulse to promote electrons in the solid from bonding orbitals to anti-bonding orbitals, thereby changing the ionic potential's coordinate of minimum energy. Because the lattice cannot respond adiabatically to this rapid displacement of the ionic equilibrium coordinate, the lattice is set into oscillation about the new equilibrium. With the DECP mechanism, the generated coherent phonon can be large enough to modulate significantly the energy bands of a solid through a deformation potential coupling.[21] Energy band modulation is manifested through transient reflectivity modulations as large as 12 percent in semiconducting Ti_2O_3 at the A_{1g} optical phonon frequency (~ 7 THz). In experiments involving high excitation intensities, it is observed that the optical phonon is screened by the photoexcited carriers, resulting in an initial down-shift of the optical phonon frequency relative to the value found through spontaneous Raman scattering.

We have recently performed coherent phonon measurements on single crystal Sb, as a function of pump intensity, to study systematically the effect of the phonon frequency shifts. These shifts are directly related to the time evolving curvature of the ionic potential caused by the pump-induced plasma. The plasma screens the bare-ion potential of the solid yielding a "dressed" phonon with a modified phonon frequency, analogous to the case of acoustic phonons in metals. By monitoring the phonon frequency, we directly measure the relaxation of the carrier-ion screening process.

In most femtosecond studies of carrier dynamics, the induced optical changes are the result of carrier distributional changes that evolve with energy and momentum loss to the lattice. In the present experiment, the induced optical changes are dominated by the lattice and we measure changes in the phonon frequency as affected by the ions' interaction with the excited carriers. In the most direct way possible, we observe electron-phonon interactions as experienced from the point of view of the lattice itself.

---

[20] T.K. Cheng, J. Vidal, H.J. Zeiger, E.P. Ippen, G. Dresselhaus, and M.S. Dresselhaus, "Mechanism for Displacive Excitation of Coherent Phonons," *Appl. Phys. Lett.* 59: 1923 (1991); H.J. Zeiger, J. Vidal, T.K. Cheng, E.P. Ippen, G. Dresselhaus, and M.S. Dresselhaus, "Theory for Displacive Excitation of Coherent Phonons," *Phys. Rev.* B45: 768 (1992).

[21] T.K. Cheng, L. Acioli, E.P. Ippen, J. Vidal, H.J. Zeiger, G. Dresselhaus, and M.S. Dresselhaus, "Modulation of a Semiconductor-to-Semimetal Transition at Seven Teraherz via Coherent Lattice Vibrations," *Appl. Phys. Lett.* 62: 1901 (1993).

1.9 Publications and Meeting Papers

Alexander, S.B., R.S. Bondurant, D. Byrne, V.W.S. Chan, S.G. Finn, R. Gallager, B.S. Glance, H.A. Haus, P. Humblet, R. Jain, I.P. Kaminow, M. Karol, R.S. Kennedy, A. Kirby, H.Q. Le, A.A.M. Saleh, B.A. Schofield, J.H. Shapiro, N.K. Shankaranarayanan, R.E. Thomas, R.C. Williamson, and R.W. Wilson. "A Precompetitive Consortium on Wide-band All-optical Networks." *J. Lightwave Technol.* 11(5/6): 714-734 (1993).

Bergman, K., C.R. Doerr, H.A. Haus, and M. Shirasaki. "Sub-shot-noise Measurement with Fiber-squeezed Optical Pulses." *Opt. Lett.* 18(8): 643-645 (1993).

Bergman, K., H.A. Haus, E.P. Ippen, and M. Shirasaki. "Squeezing in a Fiber Interferometer with a GHz Pump." *Opt. Lett.* 19: (1994).

Boivin, L., F.X. Kärtner, and H.A. Haus. "Integrable Quantum Theory of Self-phase Modulation with Finite Response Time." *Phys. Rev. Lett.* Forthcoming.

Chen, J.C., H.A. Haus, and E.P. Ippen. "Stability of Lasers Mode Locked by Two Saturable Absorbers." *IEEE J. Quant. Electron.* 29(4): 1228-1232 (1993).

Cheng, T.K., J. Vidal, H.J. Zeiger, E.P. Ippen, G. Dresselhaus, and M.S. Dreselhaus. "Displacive Excitation of Coherent Phonons." In *Ultrafast Phenomena VIII.* New York: Springer-Verlag, 1993, pp. 66-67.

Cheng, T.K., L.H. Acioli, J. Vidal, H.J. Zeiger, G. Dresselhaus, M.S. Dresselhaus, and E.P. Ippen. "Modulation of a Semiconductor-to-Semimetal Transition at 7 THz via Coherent Lattice Vibrations." *Appl. Phys. Lett.* 62: 1901-1903 (1993).

Damask, J.N., and H.A. Haus. "Wavelength-Division Multiplexing Using Channel-Dropping Filters." *J. Lightwave Technol.* 11(3): 424-428 (1993).

Damask, J.N., and H.A. Haus. "WDM System Design Using Integrated Resonant Filters." Submitted to *J. Lightwave Technol.*

Damask, J.N., H.A. Haus, and H.I. Smith. "A Deterministic Analysis of the Coherence-Degradation Effects of Stitching Errors along a DBR Grating." Submitted to *IEEE J. Quant. Electron.*

Damask, J.N., J. Ferrera, V.V. Wong, H.I. Smith, L.A. Kolodziejski, and H.A. Haus. "Limitations and Solutions for the use of Integrated QWS-DBR Resonators in WDM Applications." International Symposium on Integrated Optics Conference on Nanofabrication Technologies and Device Integration, Lindau, Germany, April 1994. Forthcoming.

Damask, J.N., V.V. Wong, J. Ferrera, H.I. Smith, and H.A. Haus. "Optical Distributed-Feedback Channel-Dropping Filters: Design and Fabrication." Invited paper, *LEOS Annual Meeting*, San Jose, California, November 1993.

Doerr, C.R., F.I. Khatri, and M. Shirasaki. "Simulation of Pulsed Squeezing in Optical Fiber with Chromatic Dispersion." *J. Opt. Soc. Am. B* 11(1): 143-149 (1994).

Doerr, C.R., H.A. Haus, E.P. Ippen, M. Shirasaki, and K. Tamura. "Additive pulse limiting." *Opt. Lett.* 19(1): 31-33 (1994).

Doerr, C.R., K. Tamura, M. Shirasaki, H.A. Haus, and E.P. Ippen. "Orthogonal polarization fiber gyroscope with increased stability and resolution." Submitted to *Appl. Opt.*

Fleischer, S.B., E.P. Ippen, G. Dresselhaus, M.S. Dresselhaus, A.M. Rao, P. Zhou, and P.C. Eklund. "Femtosecond Optical Dynamics of C_{60} and M_3C_{60}." *Appl. Phys. Lett.* 62: 3241-3243 (1993).

Hall, K.L., A.M. Darwish, E.P. Ippen, U. Koren, and G. Raybon, "Femtosecond Index Nonlinearities in InGaAsP Optical Amplifiers." *Appl. Phys. Lett.* 62: 1320-1322 (1993).

Haus, H.A. "Additive Pulse Modelocking and Kerr-Lens Modelocking." In *Ultrafast Phenomena VIII,* Eds. J.-L. Martin, A. Migus, G. A. Mourou, and A. H. Zewail. Hiedelberg: Springer-Verlag, 55: 3-7 (1993).

Haus, H.A. "Control Filters for Repeaterless Soliton Transmission." *Fiber and Integrated Optics* 12: 187-197 (1993).

Haus, H.A. "Gaussian Pulse Wings with Passive Modelocking." *Opt. Commun.* 97(3,4): 215-218 (1993).

Haus, H.A. "Molding Light into Solitons." *IEEE Spectrum* 30(3): 48-53 (1993).

Haus, H.A. "Optical Fiber Solitons, their Properties and Uses." *Proc. IEEE* 81(7): 1-13 (1993).

Haus, H.A. "Short Pulse Generation." In *Compact Sources of Ultrashort Pulses*. Ed. I. Duling. Cambridge University Press. Forthcoming.

Haus, H.A. and A. Mecozzi. "Noise of Mode-locked Lasers." *IEEE J. Quant. Electron.* 29(3): 983-996 (1993).

Haus, H.A., E.P. Ippen, and K. Tamura. "Additive Pulse Modelocking in Fiber Lasers." *IEEE J. Quant. Electron.* Forthcoming.

Haus, H.A., and F.X. Kärtner. "On the Theory of Quantum Measurement." Papar presented at *Proceedings of the Third International Workshop on Squeezed States and Uncertainty Relations*, 1993.

Haus, H.A., J.D. Moores, and L.E. Nelson. "Effect of Third-order Dispersion on Passive Mode Locking." *Opt. Lett.* 18(1): 51-53 (1993).

Haus, H.A., and J.L. Pan. "Photon Spin and the Paraxial Wave Equation." *Am. J. Phys.* 61: 818-821 (1993).

Hirayama, Y., J.H. Smet, L.H. Peng, C.G. Fonstad, and E.P. Ippen. "Observation of 1.798 μm Intersubband Transition in InGaAs/AlAs Pseudomorphic Quantum Well Heterostructures." *Appl. Phys. Lett.* 63: 1663-1665 (1993).

Hultgren, C.T., K.L. Hall, D.J. Dougherty, G. Lenz, and E.P. Ippen. "Spectal-Hole Burning and Carrier Heating Nonlinearities in Active Waveguides." *OSA Proceedings of the OSA on Ultrafast Electronics and Optoelectronics*, San Francisco, California, January 25-27, 1993; vol. 14, pp. 1-12.

Ippen, E. "Modelocking, Stabilizing, and Starting Ultrashort Pulse Lasers." In *Ultrafast Phenomena VIII.* New York: Springer-Verlag, 1993, pp. 155-159.

Kärtner, F.X., D. Dougherty, H.A. Haus, and E.P. Ippen. "Raman Noise and Soliton Squeezing." *J. Opt. Soc. Am. B.* Forthcoming.

Kärtner, F.X., and H.A. Haus. "Quantum-mechanical Stability of Solitons and the Corresondence Principle." *Phys. Rev. A* 48(3): 2361-2369 (1993).

Kärtner, F.X., and H.A. Haus. "Quantum Nondemolition Measurements and the Collapse of Wave Function." *Phys. Rev. A.* Forthcoming.

Lyubomirsky, I., M. Shirasaki, F.X. Kärtner, and H.A. Haus. "Test of Bell's Inequality with Squeezed Light from Sagnac Fiber Ring." *JEOS Part B: Quantum Opt.* Forthcoming.

Paye, J., M. Ramaswamy, J.G. Fujimoto, and E.P. Ippen. "Measurement of the Amplitude and Phase of Ultrashort Light Pulses from Spectrally Resolved Autocorrelation." *Opt. Lett.* 18: 1946-1948 (1993).

Shirasaki, M., I. Lyubomirsky, and H.A. Haus. "Noise Analysis of Mach-Zehnder Squeezer for Nonclassical Input State." *J. Opt. Soc. Am. B.* Forthcoming.

Sun, C-K., F. Vallee, L. Acioli, E. P. Ippen, and J.G. Fujimoto. "Femtosecond Investigation of Electron Thermalization in Gold." *Phys. Rev. B.* 48: 365-368 (1993).

Tamura, K., C.R. Doerr, L. Nelson, H.A. Haus, and E.P. Ippen. "Technique for Obtaining High-energy Ultrashort Pulses from an Additive-pulse Mode-locked Erbium-doped Fiber Ring Laser." *Opt. Lett.* 19: (1994).

Tamura, K., E.P. Ippen, and H.A. Haus. "Theory of Ultrashort Pulse from All-fiber Ring Laser." Submitted to *J. Opt. Soc. Am. B.*

Tamura, K., E.P. Ippen, H.A. Haus, and L.E. Nelson. "77-fs Pulse Generation from a Stretched-pulse Mode-locked All-fiber Ring Laser." *Opt. Lett.* 18(13): 1080-1082 (1993).

Tamura, K., J. Jacobson, E.P. Ippen, H.A. Haus, and J.G. Fujimoto. "Unidirectional Ring Resonators for Self-starting Passively Mode-locked Lasers." *Opt. Lett.* 18(3): 220-222 (1993).

Tamura, K., L.E. Nelson, H.A. Haus, and E.P. Ippen. "Soliton Versus Non-soliton Operation of Fiber Ring Lasers." *Appl. Phys. Lett.* 64(2): 149-151 (1994).

Ulman, M., D.W. Bailey, L.H. Acioli, F.G. Vallee, C.J. Stanton, E.P. Ippen, and J.G. Fujimoto. "Femtosecond Tunable Nonlinear Absorption Spectroscopy in $Al_{0.1}Ga_{0.9}As$." *Phys. Rev. B.* 47: 10267-10278 (1993).

1.10 Ultrashort Pulse Generation in Solid State Lasers

Sponsors

Joint Services Electronics Program
Contract DAAL03-92-C-0001
National Science Foundation
Grant ECS 85-52701
U.S. Air Force - Office of Scientific Research
Contract F49620-91-C-0091
U.S. Navy - Office of Naval Research (MFEL)
Grant N00014-91-C-0084

Project Staff

Laura E. Adams, Dr. Brett E. Bouma, Dr. Artur D. Gouvei-Neto, David Huang, Malini Ramaswamy, Morrison Ulman, Dr. Lucio H. Acioli, Dr. Joseph A. Izatt, Professor James G. Fujimoto

1.10.1 Ultrashort Pulse Generation in Solid State Lasers

The development of new laser technology for ultrashort pulse generation is directly relevant to the investigation of ultrafast phenomena in materials and devices as well as the development of high speed communications and signal processing systems. In recent years there has been a rapid growth of solid-state laser technology which has revolutionized the field of short-pulse generation. Wavelength tunable pulses with durations of less than 100 fs can now be generated using a variety of new solid state laser systems. Solid state lasers have high energy storage, high reliability, and low cost. Over the last several years, our group has been active in the development of new technologies for ultrashort pulse generation in solid state lasers. Working in collaboration with Professors Erich P. Ippen and Hermann A. Haus, we have developed a new modelocking technique called additive pulse modelocking (APM) and demonstrated it in a wide variety of systems including the $Ti:Al_2O_3$ laser as well as the diode pumped Nd:YAG and Nd:YLF lasers.[22] We have also developed theoretical descriptions of short pulse generation to explain the fundamental mechanisms for pulse shaping in lasers as well as to provide design criteria for new laser systems.[23]

Over the last year, one of the major areas of investigation has been to explore the factors which limit the shortest pulse durations that can be generated from lasers. We have explored the role of higher order intracavity dispersion in limiting the pulse duration from $Ti:Al_2O_3$ lasers and developed a novel technique for controlling third order intracavity dispersion using a thin film Gires-Tournois Interferometer. This allowed us to build a laser with independently adjustable second and third order dispersion which generated a record pulsewidth of 28 fs.[24] Subsequently, other techniques to minimize intracavity dispersion have been developed and currently 11 fs pulses can be generated directly from a Kerr-Lens-Modelocked $Ti:Al_2O_3$ laser.[25]

1.10.2 Kerr Lens Modelocking for High Power Pulse Generation in Nd:YLF

Recently a new short pulse generation technique has been developed based on the use of self-focusing (Kerr lens) effects which can produce a fast saturable absorber like action.[26] This technique is called Kerr lens modelocking (KLM) and has had a major impact on the development of third generation solid state lasers. Our group has been investigating new techniques for KLM including the development of monolithically integrated nonlinear mirrors for KLM as well as theoretical descriptions

---

[22] H.A. Haus, J.G. Fujimoto, and E.P. Ippen, "Structures for Additive Pulse Modelocking," *J. Opt. Soc. Am.* B 8: 2068 (1991); J. Goodberlet, J. Wang, J.G. Fujimoto, and P.A. Schulz, "Femtosecond Passively Modelocked $Ti:Al_2O_3$ Laser with a Nonlinear External Cavity," *Opt. Lett.* 14: 1125 (1989); J. Goodberlet, J. Jacobson, J.G. Fujimoto, P.A. Schulz, and T.Y. Fan, "Self-Starting Additive-Pulse Mode-Locked Diode-Pumped Nd:YAG," *Opt. Lett.* 15: 504 (1990).

[23] H.A. Haus, J.G. Fujimoto, and E.P. Ippen, "Structures for Additive Pulse Modelocking," *J. Opt. Soc. Am.* B 8: 2068 (1991); H.A. Haus, J.G. Fujimoto, and E.P. Ippen, "Analytic Theory of Additive Pulse and Kerr Lens Mode Locking," *IEEE J. Quant. Electron.* 28: 2086 (1992).

[24] J.M. Jacobson, K. Naganuma, H.A. Haus, J.G. Fujimoto, and A.G. Jacobson, "Femtosecond Pulse Generation in a $Ti:Al_2O_3$ Laser by Using Second and Third Order Intracavity Dispersion," *Opt. Lett.* 17: 1608 (1992).

[25] M.T. Asaki, C.P. Huang, D. Garvey, J. Zhou, H.C. Kapteyn, and M. M. Murnane, "Generation of 11 fs Pulses from a Self-Mode-Locked Ti:Sapphire Laser," *Opt. Lett.* 19: 977 (1993).

[26] D.K. Negus, L. Spinelli, N. Goldblatt, and G. Feuget, "Sub-100 fs Pulse Generation by Kerr Lens Modelocking in $Ti:Al_2O_3$," *Technical Digest of the Topical Meeting on Advanced Solid State Lasers* (Washington, D.C.: Optical Society of America, 1991), postdeadline paper.

for self-focusing nonlinearities to facilitate the design of KLM laser systems.[27]

To date, most current femtosecond laser geometries use the Kerr nonlinearity in the gain medium to obtain saturable absorber action. Our group has recently developed a new nonlinear intracavity device for passive modelocking which is called the microdot mirror.[28] The microdot mirror uses nonlinear self-focusing that occurs in a bulk intracavity element to produce fast saturable absorber modelocking. The advantages of the microdot modelocker are that it is modular, compact and independent of pump geometry and cavity design.

We have demonstrated the microdot mirror to modelock an Argon laser pumped Ti:Al_2O_3 laser.[28] Recently, we have extended the use of this novel modelocker to demonstrate KLM in a lamp-pumped Nd:YLF laser[29] to achieve pulse durations of 2.3 ps. These pulses are the shortest pulse durations that have been generated from a lamp pumped Nd:YLF laser and are close to the bandwidth limit of the Nd:YLF gain medium. According to theory, stable chirp-free generation of pulses requires both saturable absorber action and net negative dispersion. Our laser incorporated a microdot mirror modelocker for saturable-absorber action and an air-space Gires-Tournois interferometer for compact dispersion compensation. The amount of dispersion could be varied by adjusting the spacing between the mirrors in the GTI. This is, to our knowledge, the first demonstration of KLM in a lamp-pumped laser geometry. We believe that it proves the utility of the microdot-mirror technique to modelock lamp-pumped lasers and thus has important implications for the development of high power modelocked lasers.

We are currently investigating the scalability of KLM into another regime—that of compact, high rep-rate laser geometries. This effort is motivated by the need for compact, reliable and diode-pumpable femtosecond laser geometries. In current KLM laser designs, the primary hindrance to the achievement of compactness is operation in the negative dispersion regime and the consequent use of a prism pair. Another possible regime of operation which we are exploring is the positive dispersion regime, where by enhancing the saturable absorber action to self-phase-modulation ratio one can in principle achieve stable short pulse generation. Theory has shown that this requires working close to the geometrical stability limit of the laser, and we are examining the experimental validity of this concept for femtosecond laser design. A concurrent approach to the problem is the development of novel and compact ways of providing dispersion compensation using novel laser geometries.

1.11 Cavity Dumping Techniques for Modelocked Ti:Al_2O_3 Lasers

For many applications, it is desirable to generate high intensity ultrashort pulses for studies of nonlinear phenomena. Several amplification techniques have recently been developed to extend the range of available pulse energies from Ti:Al_2O_3 laser sources. However, the requirement of multiple stages and/or multiple pump lasers makes these oscillator-plus-amplifier systems complex and relatively expensive. Further, the repetition rate of many of these sources is in the kHz range and is low enough to limit detection sensitivity for ultrafast measurements.

To address these issues we have studied cavity dumping as an alternative approach to amplification for generating increased pulse energies. Cavity dumping maintains the performance advantages of modelocked Ti:Al_2O_3 lasers in terms of stability, tunability and pulse duration, while providing a significant increase in pulse peak power at variable repetition rates. We have performed what is to our knowledge the first demonstration of cavity dumping in a femtosecond Ti:Al_2O_3 laser.[30] Because solid state lasers have relatively small gain cross sections and high saturation energies, a signifcant increase in intracavity pulse energy can be achieved using high Q cavities. Our cavity dumper was an acousto-optic Bragg cell placed in an intra-

---

[27] D. Huang, M. Ulman, L.H. Acioli, H.A. Haus, and J.G. Fujimoto, "Self-Focusing Induced Saturable Loss for Laser Modelocking," *Opt. Lett.* 17: 511 (1992); G. Gabetta, D. Huang, J. Jacobson, M. Ramaswamy, E.P. Ippen, and J.G. Fujimoto, "Femtosecond Pulse Generation in Ti:Al_2O_3 Using a Microdot Mirror Mode Locker," *Opt. Lett.* 17: 547 (1992).

[28] G. Gabetta, D. Huang, J. Jacobson, M. Ramaswamy, E.P. Ippen, and J.G. Fujimoto, "Femtosecond Pulse Generation in Ti:Al_2O_3 Using a Microdot Mirror Mode Locker," *Opt. Lett.* 17: 547 (1992).

[29] M. Ramaswamy, A.S. Gouveia-Neto, D.K. Negus, J.A. Izatt, and J.G. Fujimoto, "2.3 ps Pulses from a Kerr-Lens Mode-Locked Lamp-Pumped Nd:YLF Laser with a Microdot Mirror," *Opt. Lett.* 18: 1825 (1993).

[30] M. Ramaswamy, M. Ulman, J. Paye, and J.G. Fujimoto, "Cavity-Dumped Femtosecond Kerr-Lens Mode-Locked Ti:Al_2O_3 Laser," *Opt. Lett.* 18: 1822 (1993).

cavity focus. Pulse durations as short as 50 fs with pulse energies as high as 100 nJ have been achieved at repetition rates as high as 950 kHz. The dumping process is non-resonant and does not limit the bandwidth of the laser down to the 50 fs level. The resultant peak powers of 1 MW are sufficient to permit the study of a wide range of nonlinear optical effects.

This technique should prove to be an attractive and relatively simple approach for high intensity short pulse generation for a wide range of ultrafast studies. The limitation on the available pulse energies was imposed in our system by the multiple-pulse instabilities that tend to arise at high pulse energies. Electro-optic dumping techniques, which we plan to investigate in future experiments, may be able to achieve higher pulse energies.

1.11.1 Modelocking Techniques for Transient Flashlamp Pumped Ti:Al_2O_3 Lasers

Nearly all short pulse Ti:Al_2O_3 lasers to date have been cw modelocked systems with relatively low pulse energies. Short pulse energies in the range of microjoules to millijoules can be attained using regenerative and multipass amplifier systems. Multistage chirped pulse amplification techniques can produce short pulse energies up to the joule range. While these techniques achieve excellent performance, they require multiple pump lasers for the oscillator and amplifier.

In order to develop a simple economical high peak power laser source, we have investigated modelocking in a pulsed flashlamp pumped Ti:Al_2O_3 laser. Modelocking transient systems are extremely challenging because, unlike cw lasers, the pulse energy evolves rapidly. Pioneering studies on transient modelocking were performed in flashlamp pumped Ruby and Nd:Glass lasers almost three decades ago.[31] Performances of 50 mJ, 1 nsec and 1 mJ, 50 psec, respectively, were achieved in these lasers using saturable absorber dyes whose excited state lifetimes were fast compared to the pulse durations obtained. The next generation of modelocked sources obtained shorter pulse durations in quasi cw operation with "slow" saturable absorbers using a combination of saturable absorption and saturable gain. These techniques were used in both pulsed and cw pumped configurations, eventually reaching pulse durations as short as 30 fs in the colliding pulse modelocked laser. Relatively few investigations of modelocking have been performed in flashlamp pumped Ti:Al_2O_3. Modelocking with saturable absorber dyes[32] and intracavity second harmonic generation[33] have been demonstrated and resulted in relatively long pulse durations of ~ 100 ps. With the development of new modelocking techniques based on solid-state, intracavity nonlinear modulators, it is now possible to develop high performance modelocked pulsed Ti:Al_2O_3 laser technology.

In the transient Ti:Al_2O_3 system, pre-saturation exponential growth of the pulse belies traditional modelocking techniques, since pulse energy changes dynamically in time. In addition, relaxation oscillations arise from the high gain and limit the time available for pulse shortening to just a few μs, on the order of the excited state lifetime in Ti:Al_2O_3. We have modelocked flashlamp pumped Ti:Al_2O_3 using hybrid active/passive modelocking that combines different intracavity pulse shaping mechanisms in order to obtain optimal pulse shortening during the buildup time of the transient laser pulse. Active modelocking is effective for rapidly shortening pulses which are long compared to the modulation period, while in fast saturable absorber modelocking, pulse shortening increases with increasing intensity. We have employed an acousto-optic modulator (AOM) to provide active modelocking. When the AOM is the only modelocking element pulses with durations of 100 ps can be generated. In order to further reduce the pulse duration we have employed an antiresonant semiconductor Fabry-Perot saturable absorber (AFPSA) as a cavity end mirror for fast saturable absorber pulse shaping.[34] The combined active and passive modelocking allows the production of 5 ps pulses at

---

[31] H.W. Mocker and R.J. Collins, "Mode Competition and Self-Locking Effects in a Q-Switched Ruby Laser," *Appl. Phys. Lett.* 7: 270 (1965); A.J. DeMaria, D.A. Stetser, and H. Heynau, "Self Mode-Locking of Lasers with Saturable Absorbers," *Appl. Phys. Lett.* 8: 174 (1966).

[32] S. Oda, Y. Segawa, and N. Kodama, "Passive Mode Locking of a Flashlamp-Pumped Ti:Sapphire Laser," *Jap. J. Appl. Phys.* 28: 1977 (1989).

[33] K. Hamai, K.A. Stankov, H. Jelinkova, I. Prochazka, and M. Koselja, "Mode-Locking of a Flashlamp Pumped Ti:sapphire Laser using the Frequency Doubling Nonlinear Array," paper presented at International Symposium on Ultrafast Processes in Spectroscopy, Bayreuth, Germany, 1991; *Inst. Phys. Conf. Ser.* 126, Sec. 1, pp. 59-62.

[34] U. Keller and T.H. Chiu, "Resonant Passive Mode-Locked Nd:YLF Laser," *IEEE J. Quant. Electron.* 28: 1710 (1992).

a single pulse energy of ~ 20 μJ. Extension of this work to higher pulse energies is underway. By scaling the mode size on the saturable absorber and by cavity dumping, single pulse energies in the millijoule range should be obtainable.

The hybrid modelocking technique demonstrated is not constrained to any one particular modelocking mechanism. Other fast saturable absorbers in combination with optical limiters and energy integrating nonlinearities may be used to produce picosecond pulses in the millijoule range throughout the tuning bandwidth of Ti:Al_2O_3. In addition, the excellent mode quality of this laser should allow the production of powerful blue-green and ultraviolet pulses through efficient harmonic generation.

1.11.2 Modelocking Techniques for High Power Diode Arrays

High power, picosecond pulses are of interest for optical communications and signal processing applications. The highly efficient and compact nature of semiconductor diode lasers makes these sources attractive for generating short optical pulses. Active modelocking of single-stripe diodes at high modulation frequencies can produce subpicosecond pulses. However, the power available from modelocked single-stripe diodes is limited. More power can be made available for modelocking by use of large-area diode arrays or broad-area lasers. However, the large capacitance of broad-area lasers and diode arrays makes high frequency modulation difficult, limiting the pulse widths that can be achieved from active mode locking. Another method for generating short pulses is passive mode locking with a saturable absorber created by ion implantation of one diode facet. Passively modelocked ion-implanted diode arrays have been demonstrated.[35] If, instead, the saturable absorber is independent of the laser structure, it can be custom designed for optimal saturation and recovery characteristics. Single-stripe devices have been modelocked in an external cavity using a multiple-quantum-well (MQW) saturable absorber.[36] Without external amplifiers, the maximum average power was limited to 1 mW.

It is desirable to have a source for generating high-power picosecond pulses that offers both simplicity and flexibility of design. We have developed a simple, compact, high power picosecond pulse source consisting of a 400 μm wide MQW broad-area laser and a patterned MQW sample providing both saturable absorption and spatial mode control. To our knowledge, this is the first demonstration of a hybrid mode-locked broad-area semiconductor laser with an MQW saturable absorber in an external cavity. The absorber that we have used is custom tailored for our desired absorption and is grown under conditions that ensure a fast recovery time. Our external cavity is limited to only a few optical elements including an output coupler, saturable absorber, and lenses.

Our saturable absorber is a low-temperature (LT) (≈300°C) molecular-beam-epitaxy-grown AlGaAs-GaAs MQW structure. The LT MQW structure is grown on top of a dielectric mirror stack grown on a GaAs substrate. In other diode mode-locking experiments that used a MQW saturable absorber, the GaAs substrate was removed and the absorber was epoxied to a high reflection mirror.[36] Here we have the ability to design the dielectric mirror and integrate it monolithically with the MQW saturable absorber. This approach was demonstrated previously for saturable absorber mode locking of solid state lasers.[37] Stable modelocking requires that the loss both saturate and recover faster than the gain. Previously, proton bombardment and tight focusing methods were used to speed up the recovery time of the saturable absorber. We rely on the low-temperature MBE growth to provide a fast recovery time.

Replacing a single-stripe diode laser with a broad-area semiconductor laser introduces the issue of mode control in order for light to be well focused onto the saturable absorber. We have developed a novel method for achieving this mode control. The MQW sample is patterned into microdots using a selective chemical etch. By translating the sample, we lase on dots of increasingly smaller diameter, which act as apertures, forcing the laser to operate in a few of the lowest order modes.

---

[35] J. Zarrabi, E. Portnoi, and A. Chelnokov, "Passive Mode Locking of a Multistripe Single Quantum Well GaAs Laser Diode with an Intracavity Saturable Absorber," *Appl. Phys. Lett.* 59: 1526 (1991); A. Chelnokov, J.-M. Lourtioz, and P. Gavrilovic, "Ultrashort Pulses in Diffraction-Limited Beam from Diode Laser Arrays with External Cavity," *Electron. Lett.* 29: 861 (1993).

[36] P. Smith, Y. Silberberg, and D.A.B. Miller, "Mode Locking of Semiconductor Diode Lasers Using Saturable Excitonic Nonlinearities," *J. Opt. Soc. Am. B* 2: 1228 (1985); P. Delfyett, L. Florez, N. Stoffel, T. Gmitter, N. Andreadakis, Y. Silberberg, J. Heritage, and G. Alphonse, "High-Power Ultrafast Laser Diodes," *IEEE J. Quant. Electron.* 28: 2203 (1992).

[37] U. Keller, W. Knox, and G. Hooft, "Ultrafast Solid-State Mode-Locked Lasers Using Resonant Nonlinearities," *IEEE J. Quant. Electron.* 28: 2123 (1992).

The MQW sample, which is divided into a unpatterned region and a microdot region, is mounted onto an aluminum mirror. The effects of saturable absorption and mode control are evidenced by modelocking with the Al mirror, the unpatterned MQW, and the microdot yielding pulse durations of 51, 37, and 15 ps, respectively. The 15 ps result was obtained by hybrid modelocking at 593 MHz, with average power of 9 mW, and peak power of 1 W.[38] Lasing on an $\sim 13\,\mu m$ dot yielded the best result. The largest dots provided insufficient mode control, resulting in pulses comparable to those obtained with the unpatterned MQW. The smaller-diameter dots on our sample were damaged by the etching process. Recently, we have improved our processing by moving to a microstripe geometry patterned using ion-assisted etching.

Pump-probe measurements of our MQW sample revealed a recovery time of ~ 10 ps. We believe additional pulse shortening may be realized by using a faster recovery time MQW saturable absorber produced by lower temperature growth. MQW samples grown at 200°C and 250°C are currently being investigated.

1.12 Spectrally Resolved Autocorrelation for Femtosecond Diagnostics

While the field of ultrashort pulse generation has progressed rapidly, measurement techniques for femtosecond pulses are still relatively inadequate. Currently, temporal measurement techniques, such as intensity autocorrelation, determine pulse duration by making assumptions about the pulse shape. Spectral domain measurements do not provide adequate information to retrieve the complete temporal profile. We have recently addressed this issue by developing and experimentally demonstrating a new method for the complete determination of the amplitude and phase of femtosecond pulses.[39]

Our method, called spectrally resolved autocorrelation (SRA), is both convenient and accurate and relies on a simple measurement of the spectrum of the second-harmonic generated in a conventional autocorrelation setup. A robust iterative algorithm is then used to retrieve the complex temporal amplitude of the pulse from the SRA. In contrast to other approaches, the SRA can be used to directly measure nonamplified pulses at the output of a femtosecond laser. We have demonstrated the SRA technique using our regeneratively modelocked KLM $Ti:Al_2O_3$ laser as a source of pulses. We believe that this diagnostic technique will be useful in applications such as the generation of very short pulses or pulse compression, where accurate information about the amplitude and phase of pulses is essential.

1.13 Ultrafast Phenomena in Materials and Devices

Sponsors

Joint Services Electronics Program
Contract DAAL03-92-C-0001
National Science Foundation
Grant ECS 85-52701
U.S. Air Force - Office of Scientific Research
Contract F49620-91-C-0091
U.S. Navy - Office of Naval Research (MFEL)
Grant N00014-91-J-1956

Project Staff

Igor P. Bilinsky, Malini Ramaswamy, Chi-Kuang Sun, Morrison Ulman, Professor Erich P. Ippen, Professor James G. Fujimoto

1.13.1 Femtosecond Carrier Dynamics in GaAs - AlGaAs

We have established a multidisciplinary collaborative program to investigate ultrafast dynamics in semiconductor materials and devices. Our approach incorporates state-of-the-art experimental femtosecond laser measurements and theoretical ensemble Monte Carlo simulation. The combination of experimental and theoretical studies at an advanced level has allowed us to form an accurate and detailed description of ultrafast carrier dynamics in semiconductors.

Our collaboration is based on femtosecond laser experiments performed at MIT and Monte Carlo simulations and other analysis performed at the University of Florida in Professor C.J. Stanton's solid state theory group. We expect that this

---

[38] L. Adams, E. Kintzer, M. Ramaswamy, J.G. Fujimoto, U. Keller, and M. Asom, "Mode Locking of a Broad-Area Semiconductor Laser with a Multiple-Quantum-Well Saturable Absorber," *Opt. Lett.* 18: 1940 (1993).

[39] J. Paye, M. Ramaswamy, J.G. Fujimoto, and E.P. Ippen, "Measurement of the Amplitude and Phase of Ultrashort Light Pulses from Spectrally Resolved Autocorrelation," *Opt. Lett.* 18: 1946 (1993).

project will ultimately enable us to predict the ultrafast dynamics of carriers in a wide range of semiconductors, engineered materials, and devices. This knowledge has broad reaching significance beyond fundamental interest because the carrier dynamics in a given semiconductor determine the physical limits of device speed. Since carriers scatter as fast as once every few femtoseconds, accurate models and relevant experiments must explore phenomena on a femtosecond time scale. Experimentally femtosecond pulsed lasers are required, and Monte Carlo simulation has proven to be the most effective analytical technique.

Working within this collaborative framework, we performed a study on AlGaAs using a tunable femtosecond source.[40] In this work, we developed a source of optical pulses as short as 40 femtoseconds tunable in wavelength from the red to the near infrared. We used the tunable source to excite carriers to a sequence of different initial distributions in the conduction band. Then we probed the evolution of these carrier distributions. The carrier distribution changes rapidly via carrier-carrier scattering and relaxes in energy by phonon emission. We used the mole fraction of aluminum in AlGaAs as an additional parameter to control the possible mechanisms by which the carrier distribution evolves. For example, we picked $Al_{(0.1)}Ga_{(0.9)}As$ in an effort to isolate the effects of electron intervalley scattering. Intervalley scattering is a fundamental process that is responsible for many high field transport properties in GaAs and AlGaAs. Professor Stanton's group at the University of Florida simulated our results and created a model that predicts the behavior we observed over a wide range of initial carrier energies.

A colliding pulse modelocked ring dye laser is at the heart of our apparatus. It generates optical pulses as short as 35 femtoseconds. These pulses are amplified to microjoule energies in a two stage dye amplifier that is pumped by a copper vapor laser. The amplified pulses are focused into a flowing jet of ethylene glycol to generate a femtosecond white light continuum. The continuum is then filtered in a Fourier grating filter which selects the desired wavelength and bandwidth pulse corresponding to the energy and spread in energy of photoexcited carriers. We have recently improved our system by replacing the copper vapor laser with a diode pumped, Q-switched, frequency doubled Nd:YLF laser.[41] Its all solid state design offers improved reliability and ease of use compared to the copper vapor laser.

Recently, we performed an experiment to examine the dynamics of carriers in the presence of a background cold carrier plasma.[42] This experiment approximates the conditions found in diode lasers and is complementary to the diode laser experiments described in the next section. Our experiments use 0.2 micron thick bulk samples so it is possible for us to use shorter pulses than are used in standard diode experiments where the sample is several hundred microns long and dispersion limits resolution. We use a three pulse pump-probe technique in which the third pulse, the "prepulse," is focused on the sample a few hundred picoseconds before the pump-probe measurement is performed. The prepulse is far enough ahead of the other pulses that the carriers it generates have time to cool to the lattice temperature, but not so advanced that those carriers have time to recombine. By using samples with different mole fractions of aluminum, we were able to "tune" the semiconductor instead of varying the laser wavelength. We investigated dynamics above and below the Fermi level established by the cold plasma and the effect of intervalley scattering. We found that the cold plasma increases the hot carrier thermalization rate by only a small amount and that this rate is slower than the intervalley scattering rate. We are continuing these experiments with our tunable laser system to better resolve the dynamics in energy.

The theoretical modeling of our results is undertaken in three steps. First, the semiconductor band structure is calculated. Next, the evolution of the carrier distribution function is tracked by a Monte Carlo simulation solution to the Boltzmann Transport Equation. Finally, the differential change in transmission versus pump-probe delay—the experimental results—are predicted. It is necessary to undertake this procedure in a large computer simulation because there are many optical transitions and scattering channels that must be considered. Monte Carlo simulation is the only way to extract

---

[40] M. Ulman, D.W. Bailey, L.H. Acioli, F.G. Vallee, C.J. Stanton, E.P. Ippen, and J.G. Fujimoto, "Femtosecond Tunable Nonlinear Absorption Spectroscopy in AlGaAs," *Phys. Rev. B* 47: 10267 (1993).

[41] P.C. Becker, A.G. Prosser, T. Jedju, J.D. Kafka, and T. Baer, "High-Intensity and High-Repetition Rate Q-Switched Diode-Pumped Nd:YLF-Pumped Femtosecond Amplifier," *Opt. Lett.* 16: 1847 (1991).

[42] L.H. Acioli, M. Ulman, F.G. Vallee, and J.F. Fujimoto, "Femtosecond Carrier Dynamics in the Presence of a Cold Plasma in GaAs AlGaAs," *Appl. Phys. Lett.* 63: 666 (1993).

information about the carrier distributions from our experimental data. The simulation also permits us to artificially vary the strength of various scattering mechanisms to determine the sensitivity of the data to various processes. We have found that our models accurately predict the results of our tunable experiments over the full range of initial carrier energies that we investigated.

1.13.2 Carrier Dynamics in InGaAs Strained Layer Diodes

Nonlinear gain and transient carrier dynamics in diode lasers play important roles in laser linewidth, modulation bandwidth, amplification, and short pulse generation. Picosecond and femtosecond pump probe measurements of nonlinear gain dynamics were performed in bulk GaAs, InGaAsP MQW, and InGaAs/InGaAsP strained-layer MQW amplifiers.[43] These studies have shown that non-equilibrium carrier temperature effects play a dominant role in nonlinear gain and carrier dynamics. Carrier temperature changes are caused by a number of processes including state filling produced by stimulated transitions, free carrier absorption, and two photon absorption. Previous studies[44] have shown that free carrier absorption dominates carrier heating processes. As ~ 150 fs relaxation time had been observed which was attributed to either spectral hole burning or turn on delay of free carrier heating. In addition to nonlinear gain, carrier dynamics also produce nonlinear index effects such as self phase modulation. Recently, several new experimental techniques such as bias lead monitoring,[45] time domain interferometry,[46] and heterodyne detection[47] have been developed to study carrier dynamics in waveguide device. These techniques are based on conventional single-wavelength pump-probe geometry. No multiple-wavelength pump-probe measurements have been reported.

Recently, we invented a new technique for performing independent multiple wavelength pump-probe measurement in waveguide devices.[48] The output of a Kerr lens mode-locked Ti:Al_2O_3 laser was coupled to an optical fiber for self-phase-modulation spectral broadening. Two spectral windowing assemblies, which can select frequency and pulsewidth, were used after the fiber to produce synchronous different-frequency pump and probe pulses. The pump and probe wavelength can be varied independently and thus energy relaxation dynamics can be explicitly measured. This method represents a new and powerful approach for performing ultrafast experimental studies.

Working in collaboration with investigators at MIT Lincoln Laboratory, we have performed the first carrier dynamics studies in InGaAs/AlGaAs strained-layer quantum well diode lasers. Strained-layer quantum well devices represent one of the most active and technologically promising areas of current optoelectronics device research. With epitaxial growth of nonlattice-matched materials, strained-layer materials provide an added degree of freedom to band structure engineering and device fabrication and design. High power, high efficiency, long lifetime, and low threshold current density semiconductor lasers have been achieved in the laboratory by InGaAs strained layer devices in the past few years.

The sample used for the studies is a broad-area InGaAs/AlGaAs graded-index separate-confinement heterostructure single quantum well (GRIN-SCH

---

[43] M.S. Stix, M.P. Kesler, and E.P. Ippen, "Observations of Subpicosecond Dynamics in GaAlAS Laser Diodes," *Appl. Phys. Lett.* 48: 1722 (1986); C.T. Hultgren, D.J. Dougherty, and E.P. Ippen, "Above-and Below-Band Femtosecond Nonlinearities in Active AlGaAs Waveguides," *Appl. Phys. Lett.* 61: 2767 (1992); K.L. Hall, G. Lenz, E.P. Ippen, U. Koren, and G. Raybon, "Carrier Heating and Spectral Hole Burning in Strained-Layer Quantum Well Laser Amplifiers at 1.5 μm," *Appl. Phys. Lett.* 61: 2512 (1992).

[44] C.T. Hultgren, D.J. Dougherty, and E.P. Ippen, "Above-and Below-Band Femtosecond Nonlinearities in Active AlGaAs Waveguides," *Appl. Phys. Lett.* 61: 2767 (1992); K. L. Hall, G. Lenz, E. P. Ippen, U. Koren, and G. Raybon, "Carrier Heating and Spectral Hole Burning in Strained-Layer Quantum Well Laser Amplifiers at 1.5 μm," *Appl. Phys. Lett.* 61: 2512 (1992).

[45] K.L. Hall, E.P. Ippen, and G. Eisenstein, "Bias-Leading Monitoring of Ultrafast Nonlinearities in InGaAsP Diode Laser Amplifiers," *Appl. Phys. Lett.* 57: 129 (1990).

[46] M.J. LaGasse, K.K. Anderson, C.A. Wang, H.A. Haus, and J.G. Fujimoto, "Femtosecond All-Optical Switching in AlGaAs Waveguides Using a Time Division Interferometer," *Appl. Phys. Lett.* 54: 2068 (1989).

[47] K.L. Hall, G. Lenz, E.P. Ippen, U. Koren, and G. Raybon, "Carrier Heating and Spectral Hole Burning in Strained-Layer Quantum Well Laser Amplifiers at 1.5 μm," *Appl. Phys. Lett.* 61: 2512 (1992).

[48] C.-K. Sun, H.K. Choi, C.A. Wang, and J.G. Fujimoto, "Studies of Carrier Heating in InGaAs/AlGaAs Strained-Layer Quantum-Well Diode Lasers Using a Multiple Wavelength Pump-Probe Technique," *Appl. Phys. Lett.* 62: 747 (1993).

SQW) ridge waveguide diode laser[49] with a bandgap near 960 nm. Femtosecond gain dynamics was investigated using a multiple-wavelength pump probe technique.[50] Studies were performed by fixing the pump and probe wavelength and varying the bias current so that gain, transparency, and absorption were produced at the pump wavelength. Studies demonstrate that carrier temperature changes mediated by both free-carrier absorption and stimulated transitions strongly govern transient gain dynamics. The energy of the pump wavelength relative to the transparency point determines which process dominates the transient response. In contrast to previous studies,[51] our investigations show that free carrier heating plays a much weaker role in determining carrier temperature dynamics than stimulated transition effects. Stimulated transition induced carrier cooling was observed in the absorption region which represents the first observation of carrier cooling in GaAs based devices.

In collaboration with theoretical physicists at University of Florida, Gainesville, a detailed theoretical model for gain dynamics was developed to aid in the interpretation of these results.[52] In the model, transient gain and differential transmission are computed in a multiband effective mass model for the quantum well bandstructure and optical matrix elements including biaxial strain, valence subband mixing, and polar optical phonon scattering both within and between subbands. Transient photogeneration of electron hole pairs by the pump pulses and subsequent relaxation of carriers by polar optical phonon scattering are calculated in a Boltzmann equation framework. Good agreement between the experiments and theoretical calculations were obtained, with the exception of the features seen in the experimental data from two photon absorption and spectral hole burning. We find that the dominant scattering mechanism is longitudinal polar optical phonon scattering, and stimulated transitions play an important role in carrier dynamics.

An increased understanding of the physical mechanisms of gain dynamics from carrier temperature changes is important for the design of new devices. In particular, the reduction of carrier heating has important implications for reducing parasitic gain saturature effects in short pulse modelocked laser diodes and amplifiers.

1.13.3 Nonequilibrium Electron Dynamics in Metals

Studies of interactions of free carriers between themselves and with their environment constitute one of the major problems of solid state physics. This has been addressed directly in the time domain employing femtosecond techniques both in semiconductors and metals. Of particular interest is the case of metals which display a very high electron density whose behavior can be modeled on relatively simple basis. The possibility of creating and probing a transient nonequilibrium electron population in metal with ultrashort laser pulses has been demonstrated by different groups.[53] In previous experiments, electron-electron interactions were assumed to be sufficiently fast to thermalize the electron gas on a time scale of the order or shorter than the laser pulse duration, although some deviations from an instantaneous response were observed.[54] Recent investigations using transient photoemission have demonstrated the existence of non-Fermi electron distribution with thermalization

---

[49] H.K. Choi and C.A. Wang, "InGaAs/AlGAAs Strained Single Quantum Well Diode Lasers with Extremely Low Threshold Current Density and High Efficiency," *Appl. Phys. Lett.* 57: 321 (1990).

[50] C.-K. Sun, H.K. Choi, C.A. Wang, and J.G. Fujimoto, "Femtosecond Gain Dynamics in InGaAs/AlGaAs Strained-Layer Quantum-Well Diode Lasers," *Appl. Phys. Lett.* 63: 96 (1993).

[51] C.T. Hultgren, D.J. Dougherty, and E.P. Ippen, "Above-and Below-Band Femtosecond Nonlinearities in Active AlGaAs Waveguides," *Appl. Phys. Lett.* 61: 2767 (1992); K.L. Hall, G. Lenz, E.P. Ippen, U. Koren, and G. Raybon, "Carrier Heating and Spectral Hole Burning in Strained-Layer Quantum Well Laser Amplifiers at 1.5 μm," *Appl. Phys. Lett.* 61: 2512 (1992).

[52] G.D. Sanders, C.-K. Sun, J.G. Fujimoto, H.K. Choi, C.A. Wang, and C.J. Stanton, "Carrier Gain Dynamics in InGaAs/AlGaAs Strained-Layer Single-Quantum-Well Diode Lasers: Comparison of Theory and Experiment," submitted to *Phys. Rev. B.*

[53] G.L. Eesley, "Observation of Nonequilibrium Electron Heating in Copper," *Phys. Rev. Lett.* 51: 2140 (1983); H.E. Elsayed-Ali, T.B. Norris, M.A. Pessot, and G.A. Mourou, "Time-Resolved Observation of Electron-Phonon Relaxation in Copper," *Phys. Rev. Lett.* 58: 1212 (1987).

[54] H.E. Elsayed-Ali, T.B. Norris, M.A. Pessot, and G.A. Mourou, "Time-Resolved Observation of Electron-Phonon Relaxation in Copper," *Phys. Rev. Lett.* 58: 1212 (1987).

times as long as 600 fs.[55] These results were observed in gold film for large changes of the electron temperature (of the order of 400°K) with a limited time resolution. Similar conclusions were drawn at lower laser fluence by analyzing the temperature dependence of the optically measured electron-phonon interaction time in gold and silver.[56]

In order to analyze the effect of the non-instantaneous electron-electron interaction on the optical response of a metal film, recently we have performed transient reflectivity and transmissivity measurements in the very low perturbation regime ($\Delta T \sim 3°K$).[57] In contrast to previous experiments, we develop a high sensitivity multiple wavelength femtosecond pump-probe technique. A nonequilibrium electron distribution was excited by free carrier absorption with a infrared pulse from a mode-locked $Ti:Al_2O_3$ laser with 120 fs pulsewidth and 880 nm - 1065 nm wavelength. The relaxation dynamics were followed by measuring the transient reflectivity and transmissivity using frequency doubled probe pulses in the visible, 440 nm - 532.5 nm, corresponding to the energy between the d-band and Fermi surface. This technique permits a more definitive measurement of electron dynamics by separating the effects of pump induced transitions from those monitored by the probe. In addition, by tuning of the probe wavelength, the transient electron distribution can be monitored close to Fermi surface where the optical property changes are maximum. This renders the measurement very sensitive and permits weak perturbations of the electron distribution. In this condition, the system response is linear, and the measured changes in reflectivity and transmissivity can be directly related to the electron distribution. This is in contrast to previous transient reflectivity and transmissivity measurements which probe the distribution far away from the Fermi surface and thus necessitate large perturbations of the electron gas. Experiments were performed in optically thin (200 Å) gold films, because the band structure of gold is relatively well known and electron diffusion effects can be neglected. The high stability, high repetition rate and tunability of the $Ti:Al_2O_3$ laser allows measurements at very low pump fluence inducing electron temperature changes only of the order of few Kelvins.

Measurements show evidence for non-Fermi electron distribution with an electron thermalization time of ~ 500 fs and an electron-lattice cooling time of 1 ps, independent of the laser fluence in the range of 2.5 mJ/cm^2 - 200 mJ/cm^2 (corresponding to estimated peak temperature change 3-200°K). Measurements were also performed in an optically thick sample (1200 degrees). The apparent thermalization dynamics of the electron gas is much faster and is shown to be dominated by transport effects.[58]

Recently, we developed a three-coupled rate equation model[59] based on an extension of the classical model of Anisimov.[60] The electron gas distribution changes are separated into thermalized and non-thermalized parts that are both coupled to the lattice. The diffusion in an optically thin sample is neglected. Combined with spectral lineshape analysis, the experimental data indicates the existance of a spectrally broad initial non-Fermi distribution relaxed around ~ 300 fs through the interaction with both electron gas and lattice system. The thermalization time through interaction with electron gas is on the ~ 500 fs time scale and the relaxation time through the interaction with lattice is on the ~ 1 ps time scale, separately. At energy close to the Fermi surface, long thermalization times on the order of 1 to 2 ps are observed from the reduction of the electron-electron scattering

---

55 R.W. Schoenlein, W.Z. Lin, J.G. Fujimoto, and G.L. Eesley, "Femtosecond Studies of Nonequilibrium Electronic Process in Metals," *Phys. Rev. Lett.* 58: 1680 (1987).

56 W.S. Fann, R. Storz, H.W.K. Tom, and J. Bokor, "Direct Measurement of Nonequilibrium Electron Energy Distributions in Subpicosecond Laser-Heated Gold Films," *Phys. Rev. Lett.* 68: 2834 (1992).

57 R.H.M. Groeneveld, R. Sprik, and A. Lagendijk, "Effect of a Nonthermal Electron Distribution on Electron-Phonon Energy Relaxation Process in Nobel Metals," *Phys. Rev. B* 45: 5079 (1992); C.-K. Sun, F. Vallee, L. Acioli, E.P. Ippen, and J.G. Fujimoto, "Femtosecond Investigation of Electron Thermalization in Gold," *Phys. Rev. B* 48: 12365 (1993).

58 R.H.M. Groeneveld, R. Sprik and A. Lagendijk, "Effect of a Nonthermal Electron Distribution on Electron-Phonon Energy Relaxation Process in Nobel Metals," *Phys. Rev. B* 45: 5079 (1992).

59 C.-K. Sun, F. Vallee, L. Acioli, E.P. Ippen, and J.G. Fujimoto, "Femtosecond Investigation of Electron Thermalization in Gold," *Phys. Rev. B* 48: 12365 (1993).

60 S.I. Anisimov, B.L. Kapeliovich, and T.L. Perl'man, "Electron Emission from Metal Surfaces Exposed to Ultrashort Laser Pulses," *Sov. Phys. JETP* 39: 375 (1974).

rates. The different line-shapes at different time delays reflect the lattice contribution.

The estimated electron thermalization time is comparable to the previous estimations.[61] On the basis of the very high electron density of metals, one would expect very fast electron-electron interactions. However, the interaction efficiency is considerably reduced by phase space filling which blocks most of the energetically possible interaction channels and by screening which considerably reduces the efficiency of the Coulombic interaction. An overall thermalization time of few hundred femtoseconds can be estimated on the basis of the Fermi liquid theory. Our results are significant because they provide some of the first detailed information on non-Fermi electron dynamics in metal and demonstrate new experimental techniques for their investigations.

1.13.4 Time Gated Scanning Tunneling Microscopy

Femtosecond laser technology enables the highest time resolution measurements of solid state phenomena possible today. In the past decade femtosecond lasers have progressed from specialized systems to a commercially available technology that is now widely applied in physics and chemistry. Similar development has occured in scanning probe microscopy. Since the invention of the scanning tunneling microscope in 1982 atomic resolution images of surfaces have become more and more routine every year. In our program on time resolved scanning tunneling microscopy we intend to combine the ultrafast time resolution of femtosecond lasers with the atomic spatial resolution of scanning probe microscopes. The goal is to develop an instrument that can perform highly localized measurements in four dimensions simultaneously.

In a scanning tunneling microscope (STM) a sharp metal tip is positioned a few angstroms from the surface under investigation. An electrical bias is applied between the tip and the surface. When the tip is close to the surface a small current will tunnel from the tip to the sample. The size of this current depends exponentially on the distance between the tip and the surface. In the constant current mode of operation, a feedback loop controls the height of the tip above the surface to maintain a constant tunneling current. This height is recorded as the tip is scanned across the sample and a topographic map of the surface results. In fact, the map shows the surface of constant electronic density of states, however the corrugations do not correspond directly to atomic positions.

If the tunneling current in an STM could be gated on a femtosecond time scale, it might be possible to observe nonequilibrium surface effects or perform ultrafast spectroscopy on single atoms or quantum dots. Other investigators have tried to gate the tunneling bias with photoconductive switches. Some studies have focused on the application of high speed SPM to circuit sampling.[62] Preliminary experiments of this type have reported picosecond time resolution.[63] In these experiments factors that limit the time resolution include spreading of the electrical pulse on its transmission line and the capacitance of the tip sample junction.

We are pursuing a different method of gating the tip which is based on creating a nonequilibrium carrier distribution in the tip, the sample or both. We know from our studies of hot electrons in metals and semiconductors that a photoexcited hot carrier distribution relaxes significantly within 100 femtoseconds and thermalizes in approximately 1 picosecond. We expect that tunneling will be significantly different from a hot electron distribution than from an equilibrium distribution. We are testing this concept with an equal pulse correlation technique using an amplified femtosecond laser system.

1.14 Laser Medicine

Sponsors

National Institutes of Health
Grant R01-GM35459-08
U.S. Air Force - Office of Scientific Research
Grant F49620-93-1-0301

---

[61] R.W. Schoenlein, W.Z. Lin, J.G. Fujimoto, and G.L. Eesley, "Femtosecond Studies of Nonequilibrium Electronic Process in Metals," *Phys. Rev. Lett.* 58: 1680 (1987); W.S. Fann, R. Storz, H.W.K. Tom, and J. Bokor, "Direct Measurement of Nonequilibrium Electron Energy Distributions in Subpicosecond Laser-Heated Gold Films," *Phys. Rev. Lett.* 68: 2834 (1992).

[62] A.S. Hou, F. Ho, and D.M. Bloom, "Picosecond Electrical Sampling using a Scanning Force Microscope," *Electron. Lett.* 28: 2302 (1992);. K. Takeuchi and Y. Kasahara, "High-Speed Optical Sampling Measurement of Electrical Wave form using a Scanning Tunneling Microscope," *Appl. Phys. Lett.* 63: 3548 (1993).

[63] G. Nunes, Jr., and M.R. Freeman, "Picosecond Resolution in Scanning Tunneling Microscopy," *Sci.* 262: 1029 (1993); S. Weiss, D.F. Ogeltree, D. Botkin, M. Salmeron, and D.S. Chemla, "Ultrafast Scanning Probe Microscopy," *Appl. Phys. Lett.* 63: 2567 (1993).

U.S. Navy - Office of Naval Research (MFEL)
Grant N00014-91-C-0084

Project Staff

Stephen A. Boppart, Dr. Brett E. Bouma, Michael R. Hee, David Huang, Guillermo J. Tearney, Dr. Joseph A. Izatt, Dr. Charles P. Lin, Professor James G. Fujimoto

1.14.1 Optical Coherence Tomography Technology

The development of optical coherence tomography (OCT) has led to a high-resolution imaging technology for biological tissues.[64] An incident optical beam, which is reflected or backscattered from tissue structures of varying optical density, is used to construct an image. Time delays associated with the returned light yield useful information about both the depth and reflectance of the structures. OCT is analogous to ultrasound imaging, but offers a non-invasive, non-contact system. With 10 μm resolution, OCT provides better than 10 times the resolution of current tomographic imaging technologies such as CT, MRI, and ultrasound B mode imaging.

OCT technology utilizes low coherence interferometry to obtain the depth information of the tissue. Two arms comprise the interferometer. A sample arm represents the distance to the biological tissue while the reference arm includes a translating mirror. When the optical path lengths between the two arms are matched to within the coherence length of the light source, fringes appear as an output. The translation of the reference mirror produces a 1-D depth reflectivity profile of the tissue. This interferometric ranging technique is called optical coherence domain reflectometry (OCDR).[65] Using optical heterodyne detection with the application of noise-reduction techniques originally developed for optical communication, a sensitivity of 100 dB is possible for detecting the light reflected from the tissue.

A scanning mechanism using mirrors mounted on computer-controlled galvonometers enables precise lateral positioning of the beam. Two-dimensional cross-sectional maps of the tissue backscattering magnitude are obtained when the beam is scanned in a predetermined pattern. Software routines selectively scan the beam in either a linear mode for slice images or a circular mode for circumscribing about selected tissue structures such as the optic nerve head of the eye. The data can be digitally filtered and later presented with false-color or gray scale as an optical coherence tomograph.

Our development of the OCT technology and its integration into the clinical setting has been accelerated by the strong collaborative effort between the research facilities at MIT, the Optical Communications Group at MIT Lincoln Laboratories, and the clinical facilities at the New England Eye Center of the Tufts University School of Medicine. Recent OCT advancements in the area of ophthalmology have improved the system's capabilities and ease of use. The system utilizes compact and inexpensive fiber-optic technology, including a fiber-optic interferometer, to deliver and receive the superluminescent diode laser light to and from the subject. The scanning and imaging optics have been retrofitted onto an ophthalmic slit-lamp biomicroscope to not only simplify the delivery system, but also make the technology portable and compatible with existing ophthalmic instrumentation. The 200 μW incident optical power on the retina is consistent with a conservative interpretation of the American National Standard Institute (ANSI) guidelines for safe laser retinal exposure. These guidelines have been followed throughout the development process to ensure future patient safety.

Hardware improvements have reduced the amount of time necessary for acquiring a scan. By improving the scan mechanism with the addition of a lightweight feedback controlled retroreflector and modifying the data processing circuitry and controlling software, only 2.5 s are required to obtain a 15 mm linear cross-sectional scan. This short scan

---

[64] D. Huang, E.A. Swanson, C.P. Lin, J.S. Schuman, W.G. Stinson, W. Chang, M.R. Hee, T. Flotte, K. Gregory, C.A. Puliafito and J.G. Fujimoto, "Optical Coherence Tomography," *Sci.* 254: 1178 (1991); J.A. Izatt, M.R. Hee, D. Huang, E.A. Swanson, C.P. Lin, J.S. Schuman, C.A. Puliafito and J.G. Fujimoto, "Micron-Resolution Biomedical Imaging with Optical Coherence Tomography," *Opt. Photon. News* 4: 14 (1993); E.A. Swanson, J.A. Izatt, M.R. Hee, D. Huang, C.P. Lin, J.S. Schuman, C.A. Puliafito and J.G. Fujimoto, "In Vivo Retinal Imaging by Optical Coherence Tomography," *Opt. Lett.* 18: 1864 (1993).

[65] R.C. Youngquist, S. Carr and D.E.N. Davies, "Optical Coherence-Domain Reflectometry: a New Optical Evaluation Technique," *Opt. Lett.* 12: 158 (1987); K. Takada, I. Yokohama, K. Chida and J. Noda, "New Measurement System for Fault Location in Optical Waveguide Devices Based on an Interferometric Technique," *Appl. Opt.* 26: 1603 (1987); D. Huang, J. Wang, C.P. Lin, C.A. Puliafito and J.G. Fujimoto, "Micron-Resolution Ranging of Cornea Anterior Chamber by Optical Reflectometry," *Lasers Surg. Med.* 11: 419 (1991); E.A. Swanson, D. Huang, M.R. Hee, J.G. Fujimoto, C.P. Lin and C.A. Puliafito, "High-Speed Optical Coherence Domain Reflectometry," *Opt. Lett.* 17: 151 (1992).

time reduces the likelihood of eye motion artifacts in the data as well as the patient's discomfort. Additional software improvements have provided real-time updating color displays of the acquired data. This feedback is critical for alignment procedures and necessary if specific ocular structures must be scanned.

We have also developed a high-resolution OCT system which uses the broad bandwidth of argon-pumped Ti:Al_2O_3 fluorescence. The 130 nm bandwidth of the fluorescence, centered at 790 nm, provides a coherence length down to 3 μm. This shorter coherence length should provide a three-fold increase in depth resolution. Presently, we are in the process of acquiring these higher-resolution images. Further work on this new laser source will increase the power of the fluorescence thereby reducing the acquisition time and increasing the signal-to-noise ratio of the data.

Development of the OCT system will progress toward a more clinically and patient friendly medical instrument that will not only prove to be a vital diagnosis tool for the physician, but also a multifaceted research device for the scientist. Success with this technology in both the laboratory and clinical environment has placed OCT on the verge of becoming a viable new biomedical imaging modality.

1.14.2 Optical Coherence Tomography in Ophthalmic Diagnosis

In collaboration with investigators at the New England Eye Center of the Tufts University Medical School, we have been investigating OCT as a new ophthalmic imaging instrument in both the anterior and posterior eye. Several features make OCT particularly attractive for imaging ocular tissue in comparison to existing ophthalmic examination techniques. OCT is non-contact and has superior resolution to conventional clinical ultrasound. In contrast to both scanning laser tomography and scanning laser ophthalmoscopy, the axial resolution of OCT only depends on the temporal coherence properties of the source and not on the pupil-limited numerical aperture of the eye or ocular aberrations. Micron scale axial resolution is particularly important for the early diagnosis and monitoring of degenerative retinal diseases. We have developed an OCT system which is integrated with a standard slit-lamp biomicroscope for in vivo tomography of the anterior and posterior eye.[66] OCT probe light is directed into the eye with a pair of orthogonally mounted, computer controlled galvanometric scanning mirrors, enabling arbitrary transverse scanning patterns. The probe beam focus is coincident with the slit-lamp image plane which allows simultaneous scanning and operator visualization of the eye through either the slit-lamp ocular or an attached CCD camera. For tomography of the anterior eye, the structure of interest is placed directly at the probe beam focus. Images of the posterior eye are obtained in a manner similar to indirect ophthalmoscopy, whereby a 78 diopter Volk lens placed in front of the eye is used to relay an image of the retina to the slit-lamp image plane. A computer monitor provides a real-time display of the tomograph in progress, which for retinal images is fully updated every 2.5 seconds.

In the anterior eye, the micron scale lateral and longitudinal resolution of OCT permits highly accurate biometry of large scale ocular structures, as well as the evaluation of changes in cellular morphology associated with pathologies of the cornea, iris, and lens. High sensitivity is important to detect weak backscattering from within nominally transparent structures such as the cornea and lens. We have obtained in vivo OCT tomographs of the full anterior chamber from normal human subjects.[67] These tomographs accurately profile the gross morphology of large-scale structures such as the cornea, iris, lens anterior capsule, and lens. Clinically relevant measurements may be obtained directly from these images, and include anterior chamber depth and angle, corneal thickness and curvature, and refractive power. These measurements have potential applications in contact lens fitting, post-cataract surgery intraocular lens implant power calculations, real-time monitoring of keratorefractive surgery, and the monitoring and quantification of keratitis, corneal edema, intraocular tumors, and angle-closure glaucoma.

Full-scale tomographs provide information on the large scale morphology of anterior segment structures. By narrowing the field of view, we can obtain high resolution OCT images of ocular microstruc-

---

[66] E.A. Swanson, J.A. Izatt, M.R. Hee, D. Huang, J.G. Fujimoto, C.P. Lin, J.S. Schuman, and C.A. Puliafito, "In Vivo Retinal Imaging Using Optical Coherence Tomography," *Opt. Lett.* 18: 1864 (1993); M.R. Hee, J.A. Izatt, E.A. Swanson, D. Huang, J.S. Schuman, C.P. Lin, C.A. Puliafito, and J.G. Fujimoto, "Optical Coherence Tomography for Micron-Resolution Ophthalmic Imaging," submitted to *IEEE Eng. Bio. Mag.*

[67] J.A. Izatt, M.R. Hee, E.A. Swanson, C.P. Lin, D. Huang, J.S. Schuman, C.A. Puliafito, and J.G. Fujimoto, "Micron-Resolution Imaging of the Anterior Eye with Optical Coherence Tomography," submitted to *Arch. Ophthalmol.*

ture which may provide important histopathological information concerning disease progression and the healing process in vivo. For example, in initial studies we have used OCT to evaluate the damage and healing due to laser thermokeratoplasty (LTK) of the cornea, a relatively new therapy currently under study for the treatment refractive errors of the eye.[68] An *in vivo* OCT tomograph taken one month post-operatively of an LTK treatment in a rabbit cornea shows an area of increased reflectivity clearly demarcating the radial extent and penetration depth of the thermal damage. Several important features of the healing process are also documented, including visualization of the single-cell layer endothelium and regrowth and thickening of the epithelium above the lesion.

The high resolution and high sensitivity of OCT in the posterior eye makes it uniquely suited for clinically relevant tomography of the human retina. We have produced high-resolution retinal tomographs of the foveal and optic disk regions of human subjects in vivo in under 2.5 s. In addition to providing important topographical information, such as optic disk cupping, these tomographs can discriminate the layered structure of the retina and normal anatomic variations in retinal nerve fiber layer thickness and retinal thickness.[69] These measurements demonstrate higher resolution in the posterior eye than can be obtained with any other noninvasive imaging technique, and may be directly applicable to the early, objective diagnosis and monitoring of a variety of degenerative retinal diseases, including glaucoma, macular degeneration, macular hole, and macular edema.

In collaboration with physicians at the New England Eye Center, we have recently initiated studies of macular and optic nerve head pathology with OCT in human patients. These tomographs provide the first high-resolution cross-sectional images of retinal pathology in living human patients. OCT imaging of the foveal region appears promising for the diagnosis and monitoring of macular disease. We have obtained tomographs from patients suffering from retinal detachment, retinoschisis, and macular hole. In contrast to fundus photography or flourescein angiography which both require relatively skilled interpretation, in each of these cases the cross-sectional view of the OCT tomograph permitted direct visualization of the detachment, loss of retina, or serous cavity, and allowed facile diagnosis of the pathology. OCT may also be useful for clinical imaging of the optic nerve head and peripapillary region, where quantitation of retinal and RNFL thickness is directly relevant to the early diagnosis and treatment of glaucoma. Unlike tonometry, visual field testing, or optic nerve head cupping, OCT measurements of nerve fiber layer thickness and loss may be able to provide an objective, early indicator of glaucoma onset.[70] In preliminary studies, we have profiled retinal thickness in both normal and glaucomatous eyes with tomographs taken in circular scans around the optic disk. These images show nerve fiber layer loss in patients with severe glaucoma. Additional study is required to assess whether OCT has the measurement reproducibility to quantify the small reductions in nerve fiber layer thickness that occurs early in disease progression.

We plan to continue our investigations of clinically relevant tomography with OCT in both the anterior and posterior eye. In particular, OCT is promising in the early diagnosis of macular edema and degeneration. Macular edema manifests as increased retinal thickness, which is difficult to assess with slit-lamp observation or fundus photography, and is poorly correlated with fluorescein leakage.[71] OCT can provide images of retinal thickness with micron-scale axial resolution, potentially permitting increased diagnostic sensitivity and quantitative assessment of the degree and localization of retinal thickening. The early clinical diagnosis of age-related macular degeneration, the leading cause of new blindness in the elderly in industrialized countries, depends on the detection of choroidal neovascular membranes which often form before the onset of vision loss. Although fluorescein angiography is highly sensitive to

---

[68] M.R. Hee, J.A. Izatt, E.A. Swanson, D. Huang, J.S. Schuman, C.P. Lin, C.A. Puliafito, and J.G. Fujimoto, "Optical Coherence Tomography for Micron-Resolution Ophthalmic Imaging," submitted to *IEEE Eng. Bio. Mag.*

[69] E.A. Swanson, J.A. Izatt, M.R. Hee, D. Huang, J.G. Fujimoto, C.P. Lin, J.S. Schuman, and C.A. Puliafito, "In Vivo Retinal Imaging Using Optical Coherence Tomography," *Opt. Lett.* 18: 1864 (1993); M.R. Hee, J.A. Izatt, E.A. Swanson, D. Huang, J.S. Schuman, C.P. Lin, C.A. Puliafito, and J.G. Fujimoto, "Optical Coherence Tomography for Micron-Resolution Ophthalmic Imaging," submitted to *IEEE Eng. Bio. Mag.*

[70] H.A. Quigley and E.M. Addicks, "Quantitative Studies of Retinal Nerve Fiber Layer Defects," *Arch. Ophthalmol.* 100: 807 (1982).

[71] M. Shahidi, Y. Ogura, N.P. Blair, M.M. Rusin, and R. Zeimer, "Retinal Thickness Analysis for Quantitative Assessment of Diabetic Macular Edema," *Arch. Ophthalmol.* 109: 1115 (1991): R.B. Nusenblatt, S.C. Kaufman, A.G. Palestine, M.D. Davis, and F.L. Ferris, "Macular Thickening and Visual Acuity: Measurement in Patients with Cystoid Macular Edema," *Ophthalmol.* 94: 1134 (1987).

leakage through these permeable membranes, angiography may not always accurately localize the leakage source, thus preventing the accurate delivery of photocoagulation therapy.[72] The high transverse resolution of OCT may provide a useful adjunct to angiography by pinpointing the location of the anatomic defect and aiding in the delivery of efficient therapy. These studies suggest that with further development, OCT has the potential to become a standard ophthalmic diagnostic tool for the examination of both the anterior and posterior eye.

1.14.3 Optical Coherence Microscopy

Optical coherence microscopy (OCM) is a new method for coherent confocal microsopy which uses low-coherence interferometry to enhance optical sectioning in highly scattering media. In OCM, improved confocal imaging is achieved through high detection sensitivity and high contrast rejection of out-of-focus light. OCM is an adaptation of optical coherence tomography (OCT), a technique developed in our laboratory which has recently been demonstrated for noninvasive, micron scale resolution cross-sectional imaging in the eye and other biological tissues.[73] The extension of this technique to confocal microscopy offers the potential for micron-resolution imaging deep into highly scattering media such as skin and endoscopically accessible tissues, and may make possible the development of a new form of noninvasive "optical biopsy."

The implementation of OCM combines aspects of confocal microscopy and low-coherence interferometry. In our setup, a scanning confocal microscope is implemented using a single mode optical fiber as the confocal aperture for both illumination and light collection. The confocal microscope comprises the sample arm of a single mode fiber optic Michelson interferometer, illuminated with broad bandwidth light from a superluminescent diode source. In the interferometer, light collected from the sample is combined in a fiber-optic beamsplitter with light returning from a calibrated length reference arm, generating an interferometric signal only when the distance to a scattering site in the sample matches the reference arm length to within the source coherence length (18 μm FWHM). By matching the reference arm length to the sample arm focal plane distance, image light from the focal plane is strongly selected against scattered light which has traversed other path lengths. The operation of OCM is analogous to optical heterodyne detection providing high sensitivity and high dynamic range (> 100 dB) detection of image light.

The sensitivity of the OCM to light from the focal region falls off exponentially with axial distance, rather than geometrically as in a conventional confocal microscope.[74] This rapid fall off is produced by the roughly Gaussian shape of the superluminescent diode source spectrum, which yields an exponential decay of the coherence function. This high rejection of light from outside the focal volume provides the potential for confocal imaging deep into scattering media with exponential attenuation such as biological tissues.

We have demonstrated the advantage of coherence gating for imaging absorbing structures embedded in highly scattering media in scattering phantoms as well as preliminary studies in biological tissues in vitro. High contrast two-dimensional images of absorbers placed in a highly scattering tissue phantom have been obtained, even though the backscatter signal at the absorber depth was overwhelmed by light scattered from other planes. Purely confocal images of the same sample contained no image information. Preliminary images of internal tissue microstructure have been obtained in mammalian gastro-intestinal tissues in vitro. These images illustrate delineation of epithelial and subepithelial layers in soft tissues and differentiation of collagenous and cartilagenous materials in heterogenous tissue samples.

We have developed a single-backscatter theoretical model to describe coherent confocal imaging in highly scattering media both with and without coherence gating. This model has been used to identify and predict fundamental limits to the imaging capa-

---

[72] R. Klein, B.E.K. Klein, and S.E. Moss, "Visual Impairment in Diabetes," *Opthalmol.* 91: 1 (1984); A. Scheider, A. Kaboth, and L. Neuhauser, "Detection of Subretinal Neovascular Membranes with Indocyanine Green and an Infrared Scanning Laser Ophthalmoscope," *Am. J. Opthalmol.* 113: 45 (1992).

[73] D. Huang, E.A. Swanson, C.P. Lin, J.S. Schuman, W.G. Stinson, W. Chang, M.R. Hee, T. Flotte, K. Gregory, C.A. Puliafito, and J.G. Fujimoto, "Optical Coherence Tomography," *Sci.* 254: 1178 (1991); E.A. Swanson, J.A. Izatt, M.R. Hee, D. Huang, C.P. Lin, J.S. Schuman, C.A. Puliafito, and J.G. Fujimoto, "In Vivo Retinal Imaging by Optical Coherence Tomography," *Opt. Lett.* 18: 1864 (1993); X. Clivaz, F. Marquis-Weible, R.P. Salathe, R.P. Novak, and H.H. Gilgen, "High-Resolution Reflectometry in Biological Tissues," *Opt. Lett.* 17: 4 (1992).

[74] T. Wilson and C. Sheppard, *Theory and Practice of Scanning Optical Microscopy* (London: Academic Press, 1984).

bilities of both confocal microscopy and OCM in highly scattering media. Assuming typical microscope optical parameters, predictions suggest that OCM can extend the range of confocal imaging from approximately 5 to approximately 15 scattering mean-free-paths of sample depth. This range of penetration is sufficient to permit imaging of many microstructural features near the surfaces of tissues which would be of clincal and histopathological interest.

These preliminary studies show promise for obtaining acceptable contrast confocal images up to several hundred microns deep (or up to three times the depth of confocal microscopy) for high resolution imaging in medical applications. OCM may thus provide a substantial advantage for imaging without the need for biopsy in biological tissues.

1.14.4 The Ultrashort Pulse Laser Scalpel

Successful application of short optical pulses for noninvasive cutting of intraocular structures is well established. Laser induced breakdown allows photodisruption or cutting of intraocular structures without intervening surgical incisions. To date, the majority of clinical applications of laser induced optical breakdown have utilized nanosecond pulses in the millijoule energy range and single pulse exposures.[75] However, mechanical side effects of laser induced breakdown with nanosecond sources pose potential hazards to adjacent ocular structures and tissues. Our investigations have demonstrated that significant reduction of collateral tissue damage may be achieved through the use of ultrashort pulses. These studies are part of an ongoing collaboration between investigators at MIT, the New England Eye Center of New England Medical Center Hospitals, and the Wellman Laboratories of Photomedicine at Massachusetts General Hospital.

We have studied and compared the mechanisms, scaling behavior, and tissue effects of single pulses in the nanosecond and picosecond ranges.[76] At comparable deposited energies, the damage zones resulting from optical breakdown induced by nanosecond and picosecond pulses are comparable; however, the threshold energy for breakdown is much lower for picosecond pulses, and near-threshold picosecond pulses produce greatly reduced collateral damage zones. Ultrashort pulses with high peak intensities can produce plasma-mediated ablation of transparent tissues, such as the cornea. Picosecond and femtosecond pulse durations have been demonstrated to produce much smoother excision edges and less damage to the adjacent tissue than nanosecond pulses.

Following these initial studies, we have developed a clinically viable picosecond laser scalpel based on a modelocked, Q-switched Nd:YAG laser with external pulse selection. This laser delivers single 100 picosecond duration pulses at a repetition rate variable from 3 to 1000 Hz; each pulse produces minimal collateral damage, while multiple pulses produce a cumulative incision effect. To optimize highly localized photodisruption in transparent structures using laser induced breakdown we have also developed a new laser technology based on flashlamp pumped titanium-sapphire. Flashlamp pumped solid state lasers feature higher pulse energy and lower cost compared to cw laser pumped lasers. As described in another section of this report, the present laser produces picosecond pulses with energies in the microjoule range. Picosecond pulses in the millijoule range should become available as a result of our ongoing research.

In addition to direct modelocking we are also developing a variable pulse duration, regeneratively amplified titanium-sapphire laser. A 20 fs, 80 MHz, nJ energy Kerr-lens-modelocked oscillator is being incorporated as a seed laser for chirped-pulse regenerative amplification in the flashlamp-pumped titanium-sapphire rod. The completed laser will have variable pulse duration (20 fs - 300 ps), wavelength tunable (700-1000 nm) output. Using this source, studies will be performed to correlate tissue incision and collateral injury effects with laser parameters (pulse duration, wavelength, and repetition rate). Studies will include time resolved measurements of the fundamental physical processes in optical breakdown, as well as tissue effects. Special emphasis will be placed on investigating pulse durations shorter than 100 picoseconds in order to reduce the pulse energy needed to achieve

---

[75] F. Fankhauser, P. Roussel, J. Steffen, E. Van der Zypen, and A. Cherenkova, "Clinical Studies on the Efficiency of High Power Laser Radiation upon some Structures of the Anterior Segment of the Eye," *Int. Ophthalmol.* 3: 129 (1981).

[76] J.G. Fujimoto, W.Z. Lin, E.P. Ippen, C.A. Puliafito, and R.F. Steinert, "Time Resolved Studies of Nd:YAG Laser Induced Breakdown," *Invest. Ophthal. Vis. Sci. 26:* 1771 (1985); B. Zysset, J.G. Fujimoto, and T.F. Deutsch, "Time Resolved Measurements of Picosecond Optical Breakdown," *Appl. Phys. B.* 48: 139 (1989); B. Zysset, J.G. Fujimoto, C.A. Puliafito, R. Birngruber, and T.F. Deutsch, "Picosecond Optical Breakdown: Tissue Effects and Reduction of Collateral Damage," *Las. Surg. Med.* 9: 193 (1989); D. Stern, R. Schoenlein, C.A. Puliafito, E.T. Dobi, R. Birngruber, and J.G. Fujimoto, "Corneal Ablation by Nanosecond, Picosecond, and Femtosecond Lasers at 532 and 625 nm," *Arch. Ophthalmol.* 107: 587 (1989).

optical breakdown below the 70 microjoule level used in our previous study. This system will serve as a valuable and unique tool for optimizing the localizability and incision rate for ultrashort pulse intraocular laser surgery.

1.15 EUV Laser Studies

Sponsor

MIT Lincoln Laboratory
Contract BX-5098

Project Staff

James G. Goodberlet, Martin H. Muendel, Timothy A. Savas, Marc Fleury, Sumanth Kaushik, Dr. Santanu Basu, Professor Peter L. Hagelstein

During the past several years, our group has developed an experimental facility to test new low-power "table-top" EUV and soft x-ray lasers. In last year's *RLE Progress Report,* we described the first observations of significant gain ($\alpha L \sim 3$) in Ni-like Nb at 204.2 Å. Efforts this year to improve on this result were unsuccessful, prompting us to re-evaluate our strategy for collisional lasers. The basic problem is that we require more intensity × length to achieve more gains-lengths using normal-incidence pumping; in response to this, we decided to implement a pulse-compression scheme to boost our available power by more than an order of magnitude. This conversion should be completed in the coming year. Experiments on a number of recombination lasers were performed, and these resulted in a very nice success: we observed significant gain ($\alpha L \sim 3 - 4$) for the first time in H-like B at 262 Å.

1.16 Ni-like Nb Studies

Sponsor

MIT Lincoln Laboratory
Contract BX-5098

Project Staff

James G. Goodberlet, Martin H. Muendel, Sumanth Kaushik, Dr. Santanu Basu, Professor Peter L. Hagelstein

Our first successful experiments showing gain in Ni-like Nb at 204.2 Å (see figure 1) constituted a major step forward in collisional excitation lasers, bringing down by more than two orders of magnitude the pump energy requirements per gain length for this type of laser.[77] Our initial attempts to improve upon these results led to damage to our preamplifier. After repairs, further attempts at extending our results were unsuccessful; nevertheless, these studies have suggested that we pursue a new strategy.

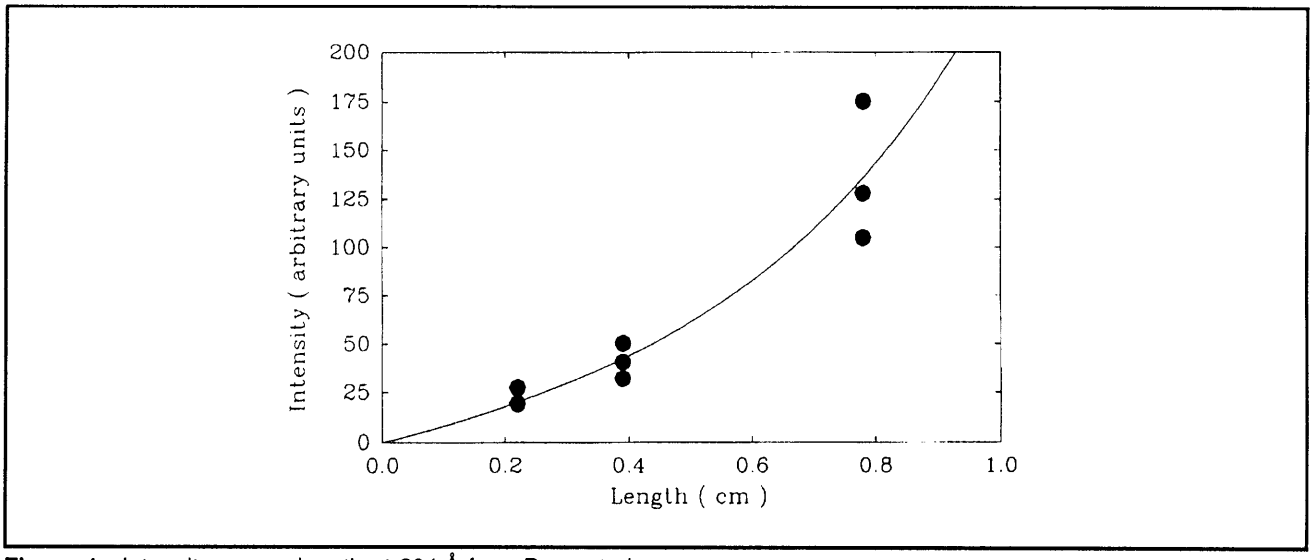

Figure 1. Intensity versus length at 204 Å from Basu et al.

[77] S. Basu, P.L. Hagelstein, J.G. Goodberlet, M.H. Muendel, and S. Kaushik, "Amplification in Ni-like Nb at 204 Å Pumped by a Tabletop Laser," *Appl. Phys. B* 57: 303-307 (1993).

After experiments at the highest power resulted in optical damage to the preamplifier, we studied our system to understand the reasons for the damage and also ways to avoid future damage. The initial results of our studies pointed to fluctuations in pulsewidth as being the prime culprit. The pulsewidth was stabilized, and new experiments were done searching for gain. The new experiments at conditions thought to be similar to our initial conditions failed to show high gain. Further experiments were done to understand what was different.

Experiments were done optimizing the line focus, varying targets between solid Nb and Nb on Si targets, varying pulsewidth, varying Z, varying the slit arrangement, and varying intensity.[78] The pulsewidth and energy were carefully measured and remeasured; the linewidth of the focus was measured to check for beam degradation.

A key observation was that there was a considerable difference in the appearance of the data between the 1992 experiments and those in 1993. The best 1992 shots gave 1 ns streak camera images that often saturated the film, with the 204.2 Å line lasting for as long as 1.3 ns. The 1993 experiments deemed to be equivalent gave 1 ns streak camera images that often needed two shots for moderate film exposure, and the 204.2 Å line never lasted longer than 0.75 ns.

It was conjectured that the energy calibration was in error in 1992 and that instead of pumping with 1 Joule per pulse, the actual energy was higher. Experiments were conducted at higher intensity and shorter lengths to attempt to verify this. At higher intensity, the experiments at shorter length became comparable in both brightness and duration of 204.2 Å emission. Consequently, we determined that the energy calibration of the 1992 experiments was low by at least a factor of 2; in retrospect, our best 1992 data was taken at more like 2 Joules/pulse!

Theory predicts that higher total gain-lengths requires more intensity × length product. In late 1992, initial experiments suggested that higher gain could be achieved at higher energy. This conjecture was tested by running at equal power with both 60 ps and at 120 ps pulses, with roughly comparable results at the two pulse intensities.

Although we were not able to improve upon our 1992 results in 1993, the results that we did get have very interesting consequences. If we could increase the pump power on target, then we should be able to increase the number of gain-lengths considerably. Our group has long considered the possibility of implementing a pulse compression scheme to increase the available energy. It is now clear that this, coupled with pulse shortening, will have a dramatic impact on the Ni-like Nb experiments.[79]

1.17 H-like Boron Recombination X-ray Laser

Sponsor

MIT Lincoln Laboratory
Contract BX-5098

Project Staff

James G. Goodberlet, Timothy A. Savas, Sumanth Kaushik, Dr. Santanu Basu, Professor Peter L. Hagelstein

One area of research on the MIT table-top x-ray laser involved a study of amplification in a recombining plasma of H-like boron. The recombination lasing scheme has been studied by several research groups in the field,[80] and gain has been demonstrated at relatively low pump energies, < 6 J for H-like carbon.[81] The spectral emission from a low Z scheme is much simpler than for a mid-Z Ni-like scheme, and data analysis is therefore simpler. Also, the ionization potential for H-like boron is about 30 percent lower than for the Ni-like Nb scheme, which would favor higher gain at lower pumping energy.

We report here a measured gain of $\alpha \simeq 3.72\ cm^{-1}$ in a recombining plasma of H-like boron. The low pumping energy, 1.1 J, and rapid firing rate, two

---

78 M.H. Muendel, *Short Wavelength Laser Gain Studies in Plasmas Produced by a Small Nd:glass Slab Laser*, Ph.D. diss., Dept. of Physics, MIT, 1994.

79 P.L. Hagelstein, "Gain Observations at 204.2 Å in Ni-like Nb," *Ultrashort Wavelength Lasers II, SPIE* 2012: 88 (1993).

80 D. Jacoby, G.J. Pert, S.A. Ramsden, L.D. Shorrock, and G.J. Tallents, *Opt. Comm.* 37: 193 (1981); D. Kim, C.H. Skinner, G. Umesh, and S. Suckewer, *Opt. Lett.* 14: 665 (1989).

81 C.H. Skinner, D. Kim, D. Voorhees, and S. Suckewer, "Development of Small-scale Soft-X-Ray Lasers: Aspects of Data Interpretation," *J. Opt. Soc. Am. B* 7: 2042 (1990).

shots per minute, of our table-top system permitted a study of the plasma gain profile. We also mounted steel blades near the target to improve gain and tested several blade designs. We found the highest gain to be 400 μm from the target surface when a blade was positioned 500 μm from the surface.

The experimental arrangement (figure 2a) has three major components. A pumping laser system, operating at 1.05 μm, produces the x-ray laser plasma which is contained in a large vacuum chamber. X-rays emitted from the plasma are detected with a streaked concave grating spectrometer (SCGS) which consists of a near normal incidence concave grating and an x-ray streak camera.

The pump laser system[82] consists of a Lumonics mode-locked Q-switched Nd:YLF oscillator which produces 20 μJ, 60 ps pulses separated by 7.5 ns. A single pulse is selected from the pulse train for amplification and beam shaping. A CCD array is used to profile the pump laser beam, and the transverse intensity profile is constant to within 20 percent across 66 percent of the $1/e^2$ beam width. Fluctuations in pulse energy and pulse duration from the oscillator were determined to be within 10 percent by monitoring fundamental and second harmonic signals as well as measuring pulse duration with a noncollinear second harmonic autocorrelator. Output from the oscillator was amplified in two stages to the 1 J level, and energy stability was determined to be within 10 percent after final amplification.

The pump beam was brought to an 8 mm length line focus on a polished solid BN target inside the vacuum chamber. The width of the line focus was measured to be 30 μm. A 100 μm x 3 mm slit was positioned 5 mm from the end of the line focus as shown in figure 2b and used to view different regions of the plasma. For most experiments, a steel blade was positioned just above the pump beam line focus as shown in the figure. Both target and blade were movable as shown. The target was translated 100 μm between shots. Plasma emission, viewed through the slit, was collected with a streaked concave grating spectrometer (SCGS) and recorded on Polaroid 667 film.

Near the target surface, a reflective steel blade was oriented to return unused pump beam radiation from the plasma back onto the original line focus (figure 2b). In addition to increasing gain via plasma cooling, we postulated that the blade might also initially heat the plasma to a higher temperature by reflecting the unused pump radiation back onto the target.

A series of experiments were performed to determine the optimal blade location and design. With the pumping energy at 1 J, we observed no gain when the blade was < 250 μm from the target surface. The 12° blade and bare target, arranged

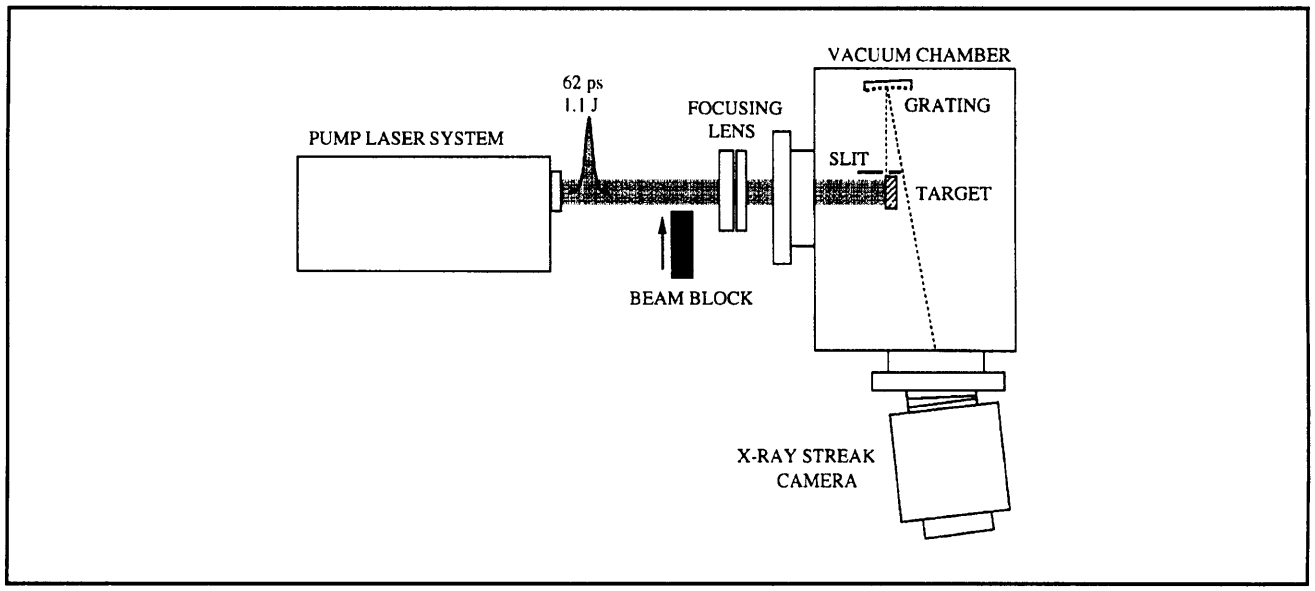

Figure 2a. The table-top XRL system. The x-ray laser is driven with an amplified, mode-locked Q-switched Nd:YLF oscillator. The pump laser beam is focused to a 30 μm wide line on the x-ray laser target.

[82] M.H. Muendel, *Short Wavelength Laser Gain Studies in Plasmas Produced by a Small Nd:glass Slab Laser*, Ph.D. diss., Dept. of Physics, MIT, 1994.

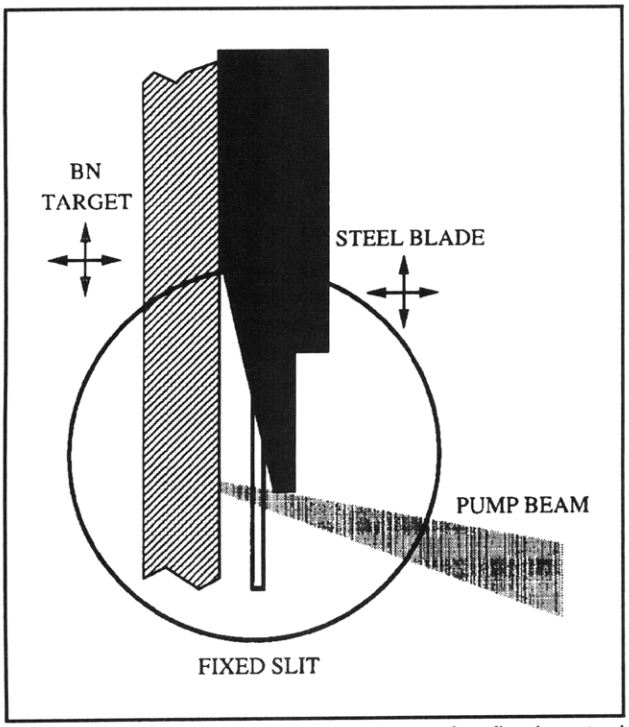

Figure 2b. The table-top XRL system. A reflective steel blade is located near the target inside the vacuum chamber. Emission from the resulting plasma is viewed through an 100 μm wide slit with a streaked concave grating spectrometer (SCGS).

as shown in figure 2b, most reliably produced gain in the plasma. With the blade properly oriented, gain values over 3 cm^{-1} were repeatedly measured.

The existence of gain was verified with several measurements. In addition to intensity versus plasma length measurements (see figures 3 and 4), gain was determined at several locations above the solid target surface for a constant surface-to-blade separation. Also, a comparison of emission from the 8 mm plasma source to emission from a point source was made (see figure 5).

Gain for the BV 3d-2p line was first determined by recording the line intensity, for an 1 ns time interval, at several different plasma lengths. The resulting line intensities at various lengths were fit to the Linford formula[83] to estimate gain.

$$I(l) \propto \exp \frac{[(\alpha l) - 1]^{3/2}}{[\alpha l \ \exp(\alpha l)]^{1/2}}$$

α is the small signal gain coefficient and l is the plasma length.

Digitized raw data from an intensity versus plasma length measurement is represented in figure 3 for four plasma lengths. The grey levels of the photos were digitally inverted for clarity. Line-outs for the spectra are also shown. The prevalent line in each photo is the 3d-2p BV line at 26.2 nm, and the weak line, noticeable in the 8 mm photo, is a NV 3s-2p line at 26.6 nm. The temporal range of each photo is approximately 1 ns. Nonlinear growth of the BV line is apparent from the raw data.

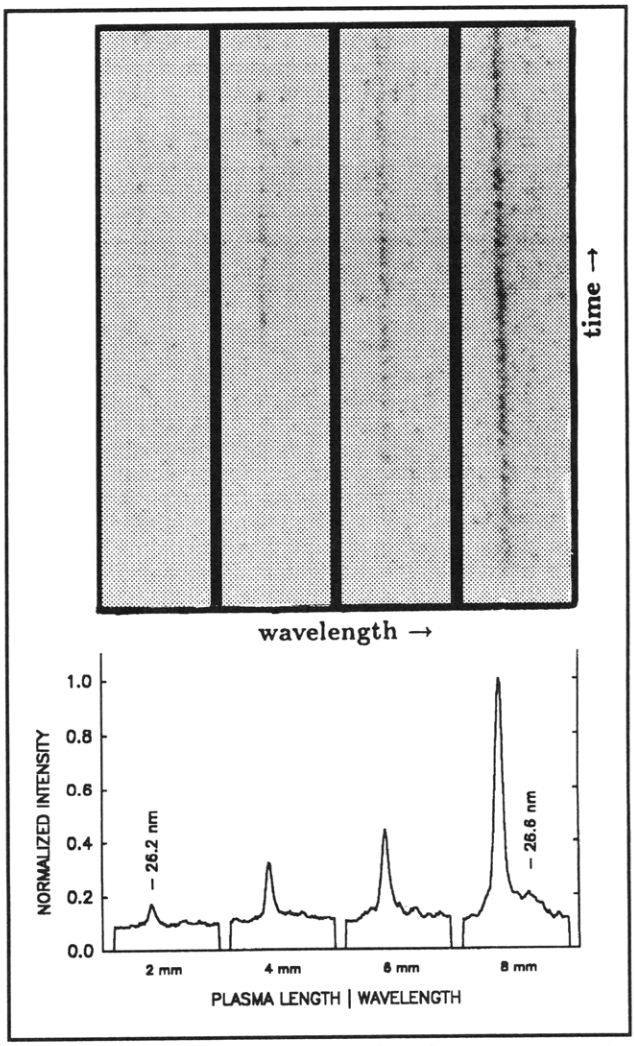

Figure 3. Intensity versus length measurements. Digitized raw data for 2, 4, 6 and 8 mm plasma lengths. The line-outs were obtained by integrating line intensities over a 600 ps time interval.

[83] G.J. Linford, E.R. Peressini, W.R. Sooy and M.L. Spaeth, *Appl. Opt.* 13: 379 1974.

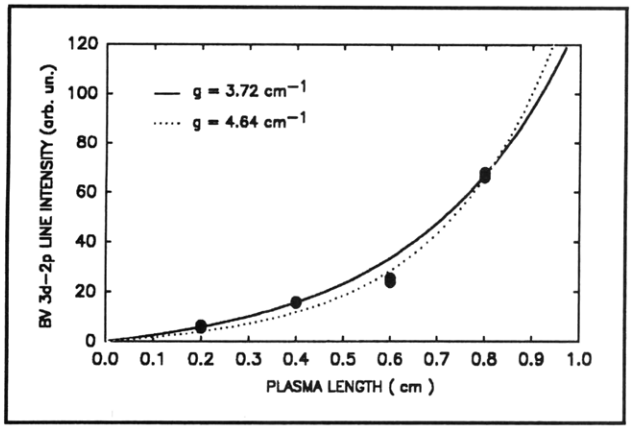

Figure 4. To estimate gain, the intensity of the BV line as a function of plasma length was fit to the Linford formula. The solid line is a fit without the 6 mm data points.

For all data points, the fit gives a small signal gain of 4.64 ± .5 cm^{-1}. When the 6 mm data points are discarded, the fit gives α = 3.72 ± .20 cm^{-1}. A data set taken several days later showed the same behavior. We believe this behavior is due to the 20 percent intensity depression at beam center, and conservatively estimate the gain to be nearer to the latter figure of 3.72 cm^{-1}.

In another experiment, gain was measured at different locations above the solid target surface. At each location, an 100 μm region of the plasma was viewed through the slit, and intensity versus plasma length measurements were made. The data, plotted in figure 6, shows an optimum region of amplification at 400 μm from the target surface. The optimum represents a compromise between an overdense, hot plasma near the target surface and a cold, underdense plasma near the blade. Such an optimum has been observed in other recombination lasers.[84]

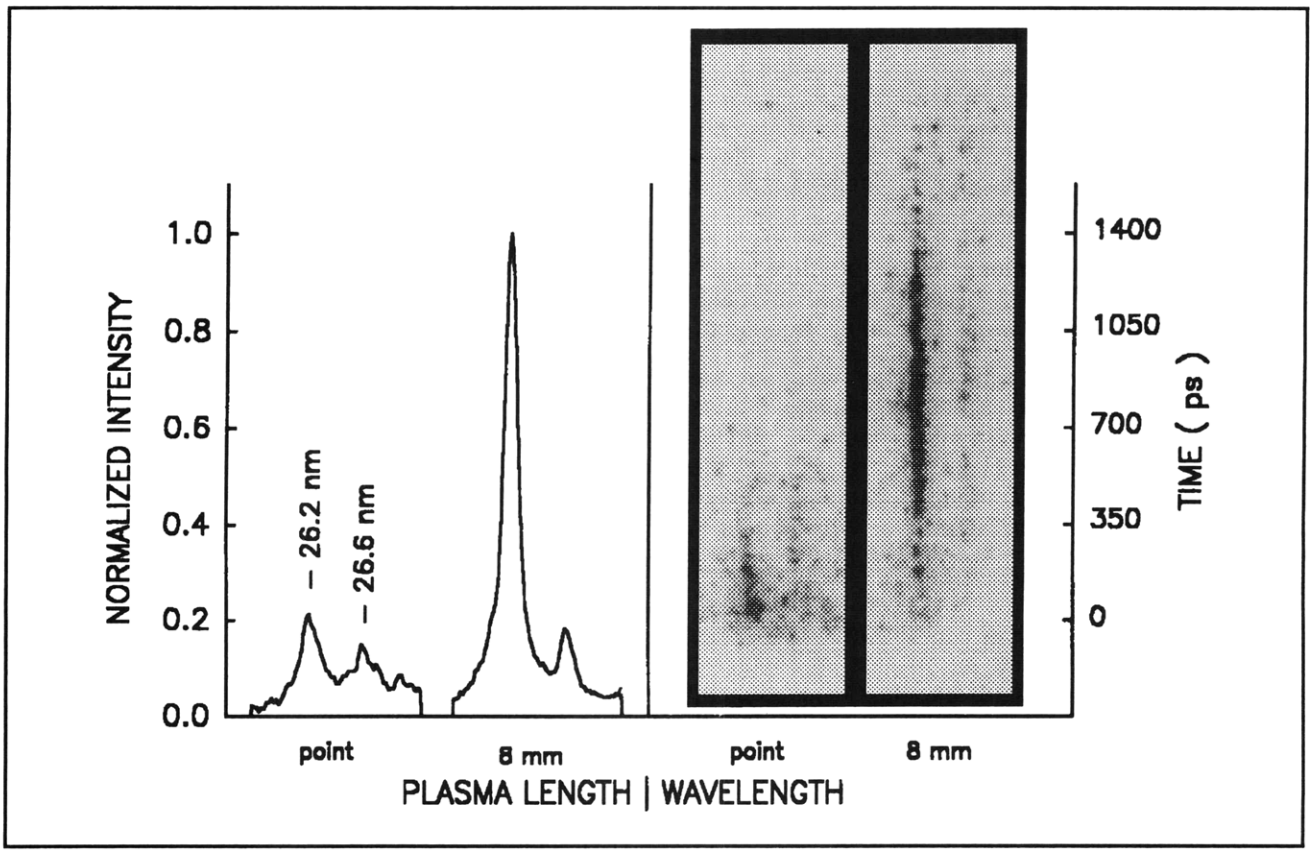

Figure 5. Point source emission versus line source emission. Emission from a point source was compared to emission from an 8 mm line source under similar pumping conditions. The substantial enhancement of the BV line suggests gain.

[84] S. Suckewer, C.H. Skinner, D. Kim, E. Valeo, D. Voorhees, and A. Wouters, "Divergence Measurements of Soft-X-Ray Laser Beam," *Phys. Rev. Lett.* 57: 1004 (1986).

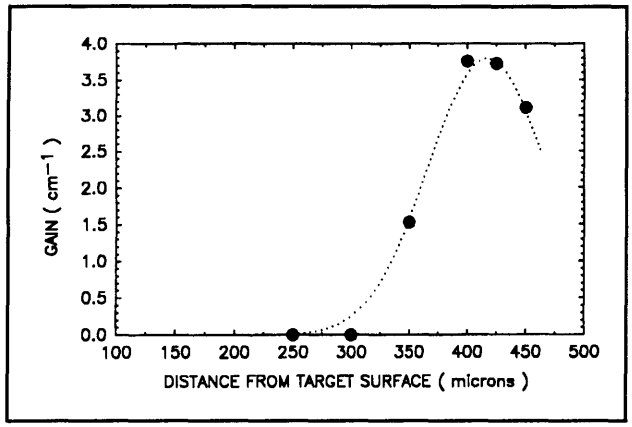

Figure 6. Gain versus distance from target. The gain was measured at several different heights above the solid target surface. The highest value of gain was recorded about 400 μm from the target surface.

1.18 Pump Laser Conversion

Sponsor

MIT Lincoln Laboratory
Contract BX-5098

Project Staff

James G. Goodberlet, Timothy A. Savas, Martin H. Muendel, Professor Peter L. Hagelstein

In order to improve x-ray laser performance, we have investigated several improvements to our pump laser system. Particularly, we have examined methods of enhanced mode-locking and chirped pulse amplification (CPA). These methods would improve the operation of our pump laser system from (1 J, ~ 60 ps) to (> 3 J, < 15 ps). Such an increase in pump energy and intensity would substantially increase the x-ray laser gain-length products. Progress in the area of pump laser conversion, to higher energy and shorter pulse, is described in the following sections.

1.18.1 Oscillator Enhancement

It has been shown that an etalon can be placed in a mode-locked cavity to shorten the output pulse.[85] The shortening is a result of bandwidth broadening of the oscillator. If the etalon's transmission minimum coincides with the peak gain wavelength of the oscillator, the net result is a broadening of the oscillator bandwidth. By adjusting the etalon thickness and angle, the curvature at gain center can be precisely cancelled.

The 150 μm thick etalon was first placed in the oscillator cavity and the output pulse duration was measured for various etalon angles. The shortest measured pulse duration was 49 ps, which compares to 68 ps without the etalon. The measurements were made with a background-free second harmonic autocorrelator and are shown in figure 7. At the angle of greatest pulse shortening, the oscillator threshold increased by ~ 40 percent.

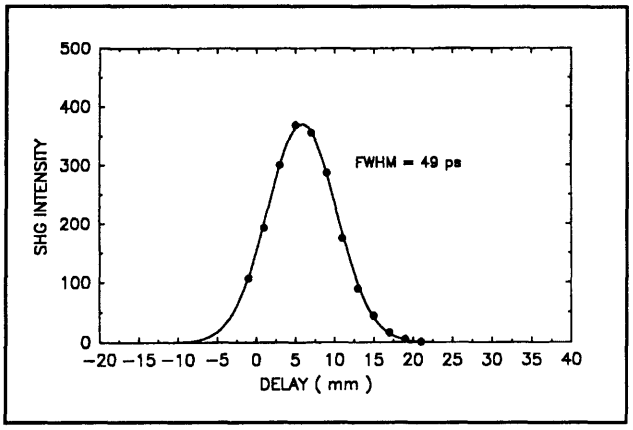

Figure 7. Pulse shortening with an intracavity etalon. An 150 μm-thick etalon was placed in the Nd:YLF oscillator to broaden the gain bandwidth and shorten the output pulse duration. The shortest pulse measured was 49 ps which represented a 28 percent pulse width reduction.

1.18.2 Chirped Pulse Amplification

A method to shorten the pump laser pulse duration and increase the pulse energy is chirped pulse amplification (CPA). This method is based upon self-phase modulation (SPM) in nonlinear material, which increases pulse bandwidth. After bandwidth broadening, the pulse is stretched before amplification and then recompressed to a shorter pulse after amplification. The pulse stretching allows higher amplification before approaching the amplifiers intensity limit. Employing this method, we anticipate achieving pump pulse energies of 3 J and duration of 15 ps.

Since self-phase modulation also gives rise to self-focusing in bulk material, the pulse bandwidth cannot be arbitrarily broadened by increasing the material length. The self-focusing distance can be increased by increasing the beam waist, but this increase will also reduce the spectral broadening

[85] M.W. McGeoch, "The Production and Measurement of Ultrashort Pulses in a Ruby Laser," *Opt. Com.* 7(3): 116 (1973).

factor. We have optimized the beam waist and material length for our input pulse duration and energy. For our system, the beam waist in the SF6 is 550 μm, and the material length is 2.3 cm.

The first phase of converting our pump laser has been to generate increased bandwidth via self-phase modulation (SPM) in bulk glass and to compress the frequency broadened pulse. Using 60 ps, 8 mJ pulses which are focused to an intensity of 10^{10} W/cm^2 in SF6 glass, we have observed spectral broadening of the pulse bandwidth by more than a factor of two and compression of the pulse duration by a factor of three. Due to unavoidable optical losses, the net increase in pump intensity presently achieved is a factor of 2.4. We anticipate an overall intensity enhancement factor of 10 after completing the conversion.

Measurements of the oscillator pulse and compressed pulse from a SHG autocorrelator are shown in figures 8a and 8b. In agreement with theory,[86] the pulse narrows and develops side lobes as the gratings are separated. The measured compression ratio is a factor of three. The measured compression ratio suggests that the pulse bandwidth has been broadened by at least a factor of three.

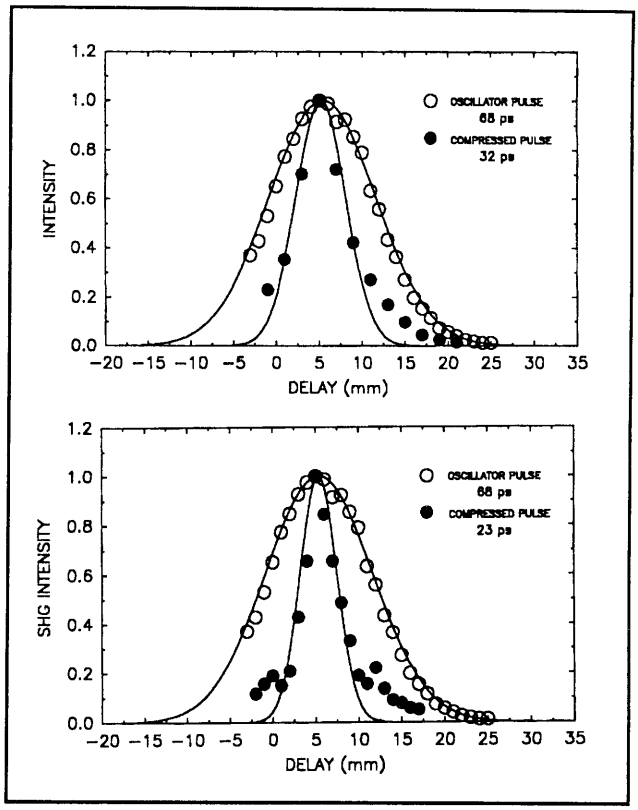

Figure 8. Compressed pulse length measurements. The pulse was measured via SHG autocorrelation after the Nd:YLF oscillator at low energy, 10 μJ, and after compression at high energy, 8 mJ. The compressor grating pair separation was 2.2 m (top) and 3.9 m (bottom) for the two measurements.

1.19 Development of a Densitometer

Sponsor

MIT Lincoln Laboratory
Contract BX-5098

Project Staff

Marc Fleury, James G. Goodberlet, Martin H. Muendel

Spectral and temporal features of our laser plasma and x-ray emissions are recorded on film in conjunction with an x-ray streak camera. Two types of film are used for our analysis: Polaroid 667 and Kodak TMZ P3200. The polaroid film has a dynamic range of 100 and is analyzed using a conventional flatbed scanner from which intensity information is obtained. The Kodak TMZ P3200 is a transparent film that has a much larger dynamic range (~ 1000). However, since it is transparent, it is not well suited for flatbed scanning. Consequently, we have designed and built a densitometer to analyze the intensity data recorded on this film.

The densitometer consists of a 5 mW He-Ne laser focused to a slit of 500 μm by 2 inches. This slit is scanned across the film using a translation stage and the transmitted light is focused and collected by a photodiode. The position of the translation stage and the intensity are read by a PC using data acquisition hardware and software. The densitometer is sketched in figure 9.

[86] W.J. Tomlinson, R.H. Stolen, and C.V. Shank, "Compression of Optical Pulses Chirped by Self-phase Modulation in Fibers," *J. Opt. Soc. Am. B* 1(2): 139 (1984).

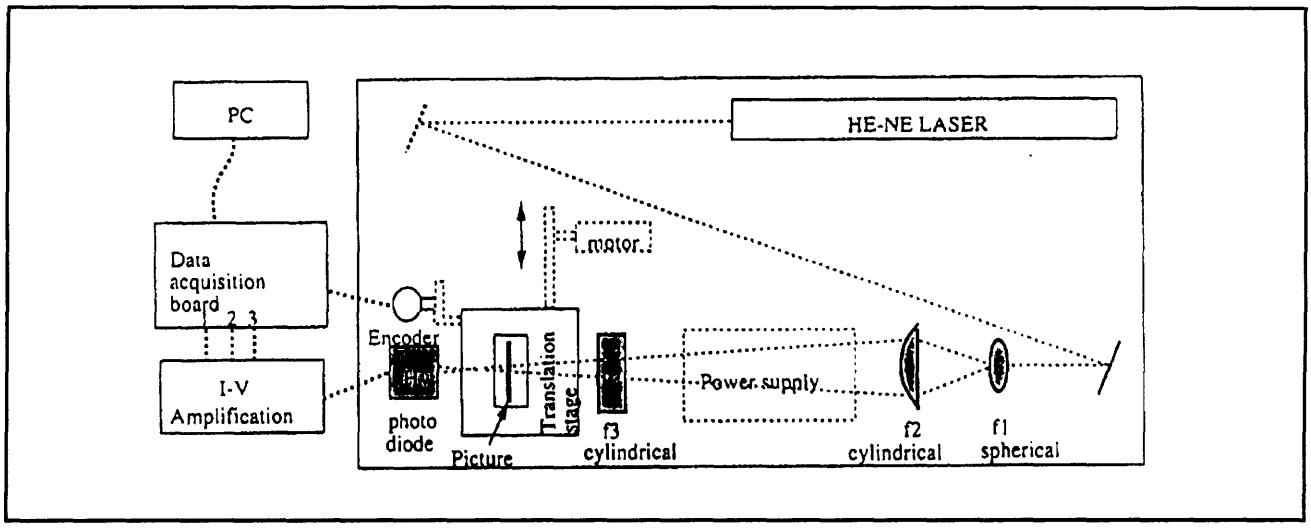

Figure 9. Schematic design of the densitometer.

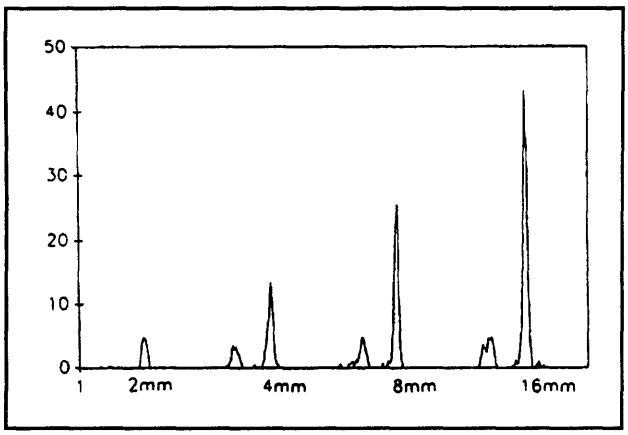

Figure 10. Intensity versus wavelength from four shots of a H-like Boron plasma.

In figure 10, we show data obtained from our densitometer. The data traces represent the intensity as a function of wavelength for emission from a H-like Boron plasma. Plotted curve is that obtained from integrating the outputs from four shots. From these curves, we have computed the dynamic range of the densitometer to be 1300 with a resolution of $\lambda/\Delta\lambda = 250$.

1.20 Quantum-Well X-ray Detector

Project Staff

Sumanth Kaushik, Professor Peter L. Hagelstein

We have designed a soft x-ray detector using multiple quantum wells that is designed to operate in the 70-500 eV range.[87] The novel feature of this proposed detector is that it is based on optical effects, which have the potential to lead to excellent sensitivity and good spatial, temporal, and energy resolutions. The detector characteristics are summarized in table 1. For energies greater than 500 eV, the detector's energy resolution deteriorates, but its other features remain essentially unaltered. This kind of detector is presently unavailable; the development of such a device would have important applications in the areas of x-ray microscopy and plasma diagnostics.

The detector (see figure 11) is based on the concept of optically imaging the x-ray induced free-carriers in semiconductor quantum wells. The general idea is to select a probe beam tuned near the onset of the heavy hole excitonic peak where the change in the optical susceptibility is the largest. The lengths of the various layers are chosen in such a manner that under quiescent conditions, the reflection is near minimum (typically 5 to 10 percent). The presence of x-ray induced carriers modifies the optical susceptibility, thereby modulating the optical impedance of the multiple-

[87] S. Kaushik, *Design and Applications of a Soft X-Ray Detector Using GaAs Multiple Quantum Wells,* Ph.D. diss., Dept. of Electr. Eng. and Comput. Sci., MIT, 1994.

quantum-well (MQW) structure.[88] The modulation in the impedance appears as reflected light and is imaged on a CCD (charged coupled device) camera. By exploiting the natural resonances in the transmission and reflection coefficients in a multilayer dielectric stack, contrast ratios as high as 10 to 20 percent can be achieved.

Design Parameters		
Parameter	Value	Tolerance
L_b : Al_xGaAs_{1-x}	50Å	± 2.4Å
L_w : GaAs	170Å	± 2.4Å
L_s : Al_xGaAs_{1-x}	48.6 nm*	± .5 nm
λ_p	818.55 nm	± 1 nm
θ_{in}	0°	± 5°
T	150 K	10 K
Detector Performance		
Spatial Resolution:		1μ
Temporal Resolution:		20 ps
Sensitivity:		25 photons/μm^2
Energy Resolution:		85 eV
Contrast Ratio:		~ 10%

Table 1. Summary of the chief parameters and performance of the detectors. The definitions of the variables are found in the text. Note: Actual L_s values can also be half-integer multiples of the probe wavelength added to the minimum value specified above.

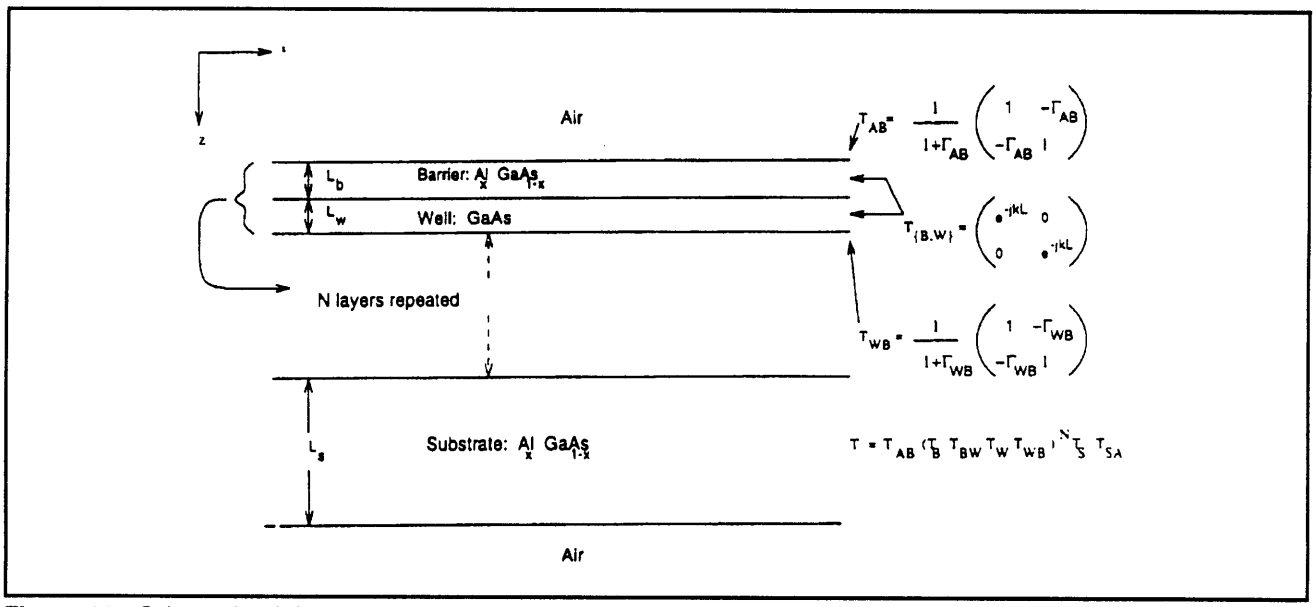

Figure 11. Schematic of the multilayer stack. With each interface and layer, a transmission matrix is associated. The overall transmission matrix is expressed as a product of individual matrices. The cap layers, usually GaAs, prevent the oxidation of the surface and are typically very thin (~ 100 Å) and do not affect the optical properties of the quantum wells significantly.

[88] S. Kaushik and P.L. Hagelstein, "A Semi Empirical Lineshape Model for GaAs MQW Structures," *IEEE J. Quant. Electron.*, forthcoming.

1.21 Lineshape Theory

We have studied the origin of non-Lorentzian features in the absorption lineshapes of excitonic transitions in semiconductors. One very pronounced feature of the absorption lineshape is that for energies well away from the resonance, the lineshape is found to decrease exponentially as a function of energy. This result, known as the Urbach's rule,[89] was first observed experimentally, and is attributed to interaction of excitons with LO-phonons.[90]

The principal result of our investigation is a new lineshape function that accounts for the interactions with LO phonons. Specifically, we have found that the lineshape function can be written as

$$\Delta(E) = \frac{2\Gamma_0 t_0}{\sqrt{\Gamma_0 + t_0^2}} e^{\Gamma_0 t_0} K_1\left[t_0(E^2 + t_0^2)^{1/2}\right] \qquad (1)$$

where

$$t_0 = \frac{\Gamma_0}{\Sigma_{\lambda q}|M_{\lambda 0}(q)|^2} \qquad (2)$$

The function K_1 is the Bessel function of the second kind. The parameter Γ_0 is the Lorentzian linewidth as measured or as computed using standard linewidth formulas.[91] The parameter $M_{\lambda 0}(q)$ is the phonon matrix element between the 1 s exciton ground state and the excited state.[92]

This lineshape function has the important property that it is Lorentzian near the resonance energy and decreases exponentially in energy for energies well away from the resonance (see figure 12). That is for $t_0(E^2 + \Gamma_0^2)^{1/2}$ small:

$$\Delta(E) \sim \frac{2\Gamma_0}{\Gamma_0^2 + E^2} \qquad \text{(Lorentzian)}$$

whereas, for $t_0(E^2 + \Gamma_0^2)^{1/2}$ large:

$$\Delta(E) \sim e^{-t_0 E}. \qquad \text{(Urbach)}$$

This exponential dependence appears to be in agreement with the well known Urbach's rule. Although the exponential tail has been shown analytically to be a consequence of exciton-phonon interaction, the earlier arguments were based on studying asymptotic properties of the Green's functions.[93] A simple analytical lineshape function of the form given in equation (1) has been hitherto lacking.

Our result is derived by writing the Green's function in the form

$$G(t) = -i\theta(t)\exp(F(t)) = -i\theta(t)\exp(\Gamma(t) - i\Sigma(t)) \qquad (3)$$

where the function F(t) is derived using cluster expansion method.[94] By noting the following very important property of $\Gamma(t)$ and $\Sigma(t)$ under time inversion

$$\Gamma_{\pm}(t) = \Gamma_{\pm}(-t)$$

$$\Sigma_{\pm}(t) = -\Sigma_{\pm}(-t) \qquad (4)$$

the functions $\Gamma(t)$ and $\Sigma(t)$ can be approximated rather accurately. The Green's function is Fourier transformed to yield the lineshape quoted in (1).

1.22 Lattice-induced Reactions

Sponsor

Electric Power Research Institute
Contract RP3170-25

---

89 F. Urbach, *Phys. Rev.* 92: 1325 (1953).

90 S. Kaushik and P.L. Hagelstein, "An Analytical Solution of the 2D Exciton-Phonon Matrix Element," *J. Math. Phys.* 35: 1021 (1994); S. Rudin and T.L. Reieneche, "Temperature Dependent Exciton Linewidths in Semiconductor Quantum Wells," *Phys. Rev. B* 41: 1017 (1990).

91 S. Rudin and T.L. Reieneche, "Temperature Dependent Exciton Linewidths in Semiconductor Quantum Wells," *Phys. Rev. B* 41: 1017 (1990).

92 S. Kaushik and P.L. Hagelstein, "An Analytical Solution of the 2D Exciton-Phonon Matrix Element," *J. Math. Phys.* 35: 1021 (1994).

93 G.D. Mahan, "Phonon-Broadened Optical Spetra: Urbach's Rule," *Phys. Rev.* 145: 602 (1960).

94 D. Dunn, "Electron-Phonon Interactions in an Insulator," *Can. J. Phys.* 53: 321 (1975).

Project Staff

Ziad J. Azzam, Sumanth Kaushik, Professor Peter L. Hagelstein

We have pursued mechanisms through which large energy transfer between a lattice and nuclei can occur. Energy transfer through conventional recoil mechanisms is well-known and does not lead to any new anomalous effects.

We investigated anomalous energy transfer through phonon mode frequency shifts in the case of neutron transfer reactions,[95] and found that associated with a mode frequency shift of $\delta\omega$, there was a corresponding energy transfer of

$$\Delta E = N\hbar\omega$$

where N is the number of phonons in the modes that shift. In the case in which the phonon modes jump across a band gap, the energy exchange per phonon can be on the order of a few meV. In the case in which the phonon mode is a continuum mode, the number of phonons can in principle be very great, resulting in anomalously large energy transfer. For example, if somehow 10^8 phonons were initially in a gap-jumping mode, the total energy transfer could be as large as fractions of an MeV.

Recently, we have generalized this basic mechanism to the case of gap-jumping between impurity phonon bands due to host vacancies in metal hydrides.[96] For example, in the case of PdH, it is known that the basic octohedral distribution of hydrogen atoms around a Pd atom within a unit cell is preserved in the presence of a Pd vacancy.[97] In this case, the hydrogen atoms see a considerably softer potential, and we speculate that this leads to impurity phonon modes within the band gap. If this is true in the case of a PdD lattice, as illustrated in figure 13, then some rather interesting physics could result.

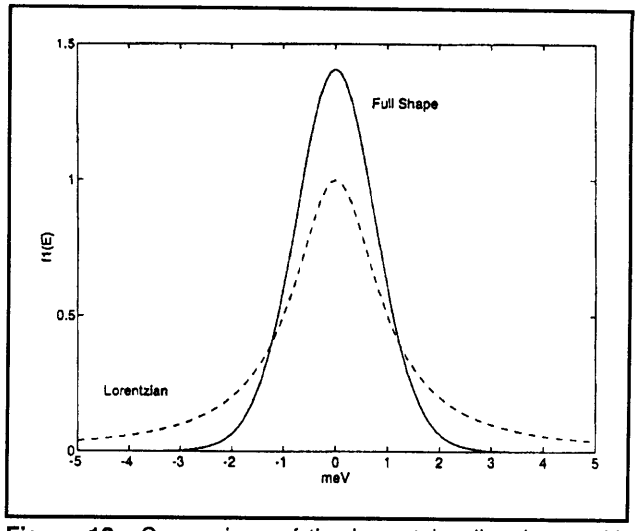

Figure 12. Comparison of the Lorentzian lineshape with the new lineshape described in the text.

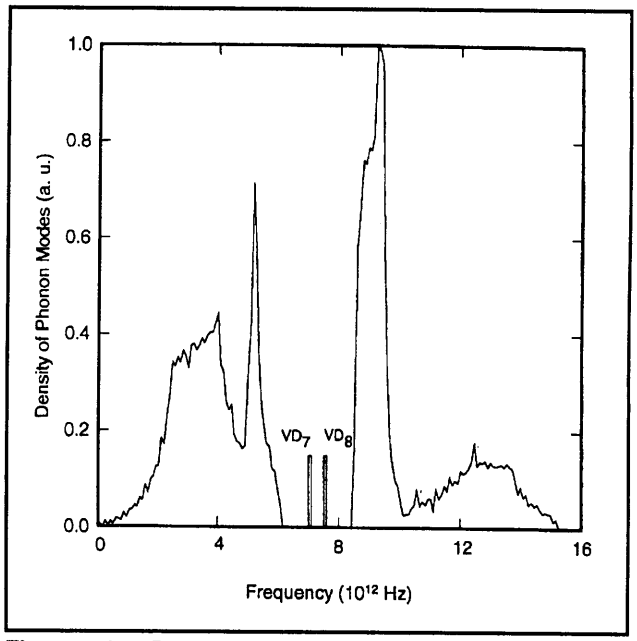

Figure 13. Density of states in PdD, augmented with proposed vacancy impurity bands (VD_7 and VD_8). VD_8 indicates modes due to cells with 8 deuterons around a Pd vacancy; VD_7 indicates modes due to 7 deuterons around a Pd vacancy.

---

[95] P.L. Hagelstein, "Coherent and Semi-Coherent Neutron Transfer Reactions I: The Interaction Hamiltonian," *Fusion Tech.* 22: 172 (1992); P.L. Hagelstein, "Coherent and Semi-Coherent Neutron Transfer Reactions III: Phonon Frequency Shifts," *Fusion Tech.* 23: 353 (1993); P.L. Hagelstein, "Possible Mossbauer Effect in Neutron Capture," presented at *International Conference on Applications of the Mossbauer Effect,* Vancouver, Canada, August 1993.

[96] P.L. Hagelstein, "Lattice-Induced Atomic and Nuclear Reactions," *Proceedings of the Fourth International Conference on Cold Fusion,* Maui, Hawaii, December 1993.

[97] Y. Fukai and N. Okuma, "Evidence for Copious Vacancy Formation in Ni and Pd under a High Hydrogen Pressure," *Jpn. J. Appl. Phys.* 32 L1256 (1993).

In this case, any process that creates a host lattice vacancy, or else changes the number of deuterons around a host lattice vacancy, will cause a change in the number of phonon modes in each impurity band. Large excitation of these modes will result in anomalous energy transfer associated with vacancy production. We have formulated a theory for this process and computed rates for a variety of decay channels.

For example, if the lowest optical phonon modes were very highly excited, then the production of a Pd vacancy would down-shift the highly excited modes, leading to energy transfer from the lattice to whatever mechanism causes the vacancy. In this case, the lattice energy can drive reactions that cause a vacancy to be produced. A dominant decay channel at large energy transfer is fast electron production, mediated by the Coulomb interaction between the nuclei and K-shell electrons. The decay rate can be calculated directly from

$$\Gamma = \sum_f \sum_k \frac{2\pi}{\hbar} | < L_i, 1s | \frac{Ze^2}{r_{12}} | L_f, k > |^2$$

$$\delta(E_f^{(L)} + \hbar^2 | k |^2/2m_e + I_K - E_i^{(L)})$$

Performing the integration over electronic coordinates leads to

$$\Gamma = \frac{2\pi}{\hbar} \sum_f \sum_k | V(k) |^2 | < \Psi_i^{(L)}(q_i) | e^{-i\hat{S}_D} e^{ik \cdot R_j} | \Psi_f^{(L)}(q_i) > |^2$$

$$\delta(I_K + \hbar^2 | k |^2/2m_e + E_f^{(L)} - E_i^{(L)})$$

where V(k) describes the Coulomb interaction

$$V(k) = Ze^2 \left[\frac{N_{1s}}{V} \right]^{\frac{1}{2}} \left[\frac{Z^3}{\pi a_0^3} \right]^{\frac{1}{2}} \frac{4\pi}{| k |^2 + (Z/a_0)^2}$$

The conventional recoil is accounted for through the appearance of $e^{ik \cdot R_j}$, and e^{-iS_D} is a Duschinsky operator that includes the effects of changes in the structure of the phonon modes.

Since only a few modes jump a band gap, these modes can be used to evaluate the Duschinsky matrix element approximately in the absence of recoil; this leads approximately to

$$\Gamma = \frac{2\pi}{\hbar} \sum_f \sum_k | V(k) |^2 | < \Psi_i^{(L)}(q_i) | e^{ik \cdot R_j} | \Psi_f^{(L)}(q_i) > |^2$$

$$\delta(I_K + \hbar^2 | k |^2/2m_e - N\hbar\delta\omega)$$

in the limit that the recoil has been sufficiently strong to create a new vacancy. If the anomalous energy transfer is large, then the recoil energy can be neglected, and the net effect of the recoil term is to determine what fraction of the time a new vacancy is created. If the probability of vacancy creation is $| T(k) |^2$, we obtain the final result

$$\Gamma = \frac{24N_{1s}}{\pi Z} \frac{I_H}{\hbar} \left[\frac{\varepsilon}{I_H} \right]^{\frac{1}{2}} \frac{1}{[1+(\varepsilon/Z^2 I_H)]^2} | T(k) |^2$$

where $\varepsilon = N\hbar\delta\omega - I_K$. This is plotted below in figure 14 for recoils from Pd and in figure 15 in the case of recoils from D.

These rates are observed to be quite fast. They are sufficiently rapid that it is *a priori* difficult to understand how such large phonon mode populations could build up in the presence of such fast reaction rates, especially if other decay modes are present that turn on at lower energy. Our picture is that many phonon modes are excited; modes not immediately next to the band gap can build up without the same limits as the lowest modes. When the lowest modes jump, they reveal new lowest modes which in turn may jump; these new modes may be quite highly excited, resulting in the possibility of large energy transfer. The associated rates as calculated by Fermi's Golden Rule are too large to be physical, implying that the decays will occur in bursts as a high-order Raman-type process.

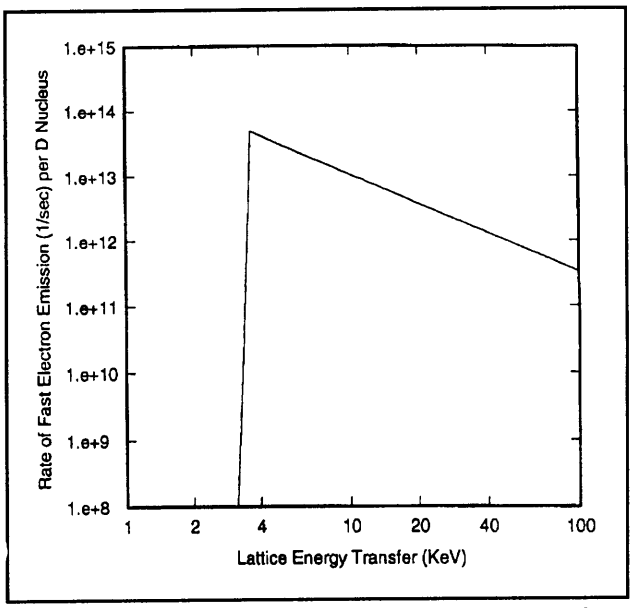

Figure 14. Predicted fast electron emission rate from deuterons as a function of lattice energy transfer.

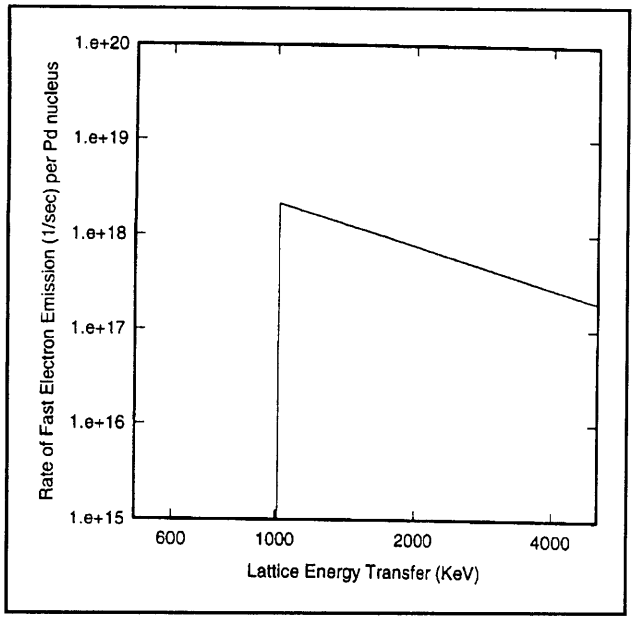

Figure 15. Predicted fast electron emission rate from Pd nuclei as a function of lattice energy transfer.

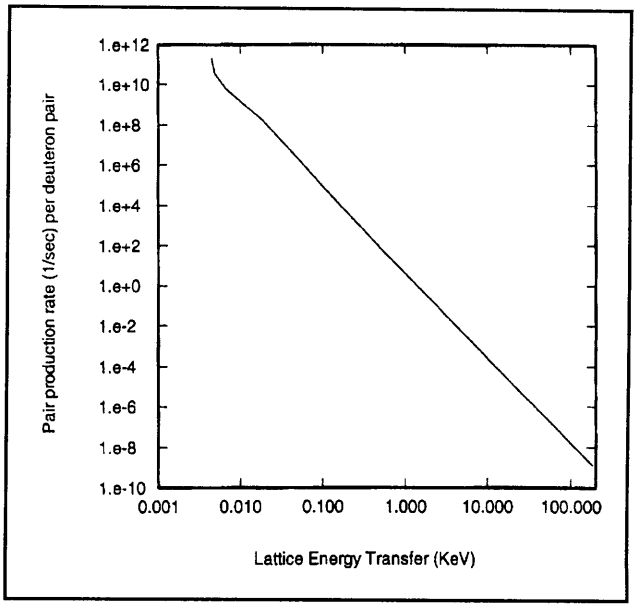

Figure 16. Decay rate per deuteron pair next to a Pd vacancy for lattice-induced Coulomb recoil.

Of immediate interest are the decay rates for Coulomb-induced deuteron-deuteron recoil (shown in figure 16), which is a dominant decay mechanism up to a few KeV of lattice energy transfer. This process results in the production of fast deuterons, up to energy transfer where fast electron decay as described above turns on. This is interesting because these deuterons are sufficiently energetic to cause fusion reactions to occur. The fusion rate per deuteron pair is shown in figure 17; these rates are observed to be sufficiently high to account for the observation of *dd*-fusion neutrons claimed to have been observed in cold fusion experiments during the last few years.

The reactions described above are based on the premise that a very large number of phonons can be developed in a single phonon mode. The situation is much like the difference between broad band light from a hot thermal source, and the radiation field inside a laser cavity. The presence of photon gain inside the laser cavity results in the development of very large photon populations in a single mode. The laser amplifier will add photons preferentially to modes within the gain linewidth that already have the most photons.

One way to generate large phonon populations in phonon modes is to create a phonon amplifier that will drive a "phonon laser". Phonon lasers have been built, but they have not operated previously in optical phonon modes. We are considering a novel mechanism to drive a phonon amplifier. If exothermic chemical reactions were to occur at a solid surface (at an interface with a gas or solid), and if the reactions involved an inhibiting potential barrier that phonons could help to overcome, then the reactions would tend to couple energy preferentially into the phonon modes that helped to stimulate the reaction. If the end product of the reaction were not stable at the surface, then a population inversion would be developed between the reactants and their products; this is the condition for phonon gain.

One interesting example of this mechanism is hydrogen desorption from a metal hydride. Absorbed and adsorbed hydrogen in metal hydrides is often localized as single atoms in local wells that occur in pockets between host lattice atoms. Gas desorption involves the tunneling of the hydrogen atoms to the bound molecular state away from the metal surface, where it is free to leave. In PdD, deuterium desorption is exothermic at very high D to Pd loading, which is where the anomalies are thought to occur.

In previous RLE reports, we have described at length novel neutron transfer reaction mechanisms. We would do so here as well, except that our report is already much too long. During the last year we have found that our model is very closely related to the Anderson model in condensed matter physics, that it can be solved approximately using perturbation theory, and that the reaction rates for the specific E1 and M1 transfer mechanisms described last year are too small to be observable. The reason that the rates are too small is that the electromagnetic coupling is very weak. A modified version of the theory that uses strong interaction neutron matrix elements, which in fact are a much closer

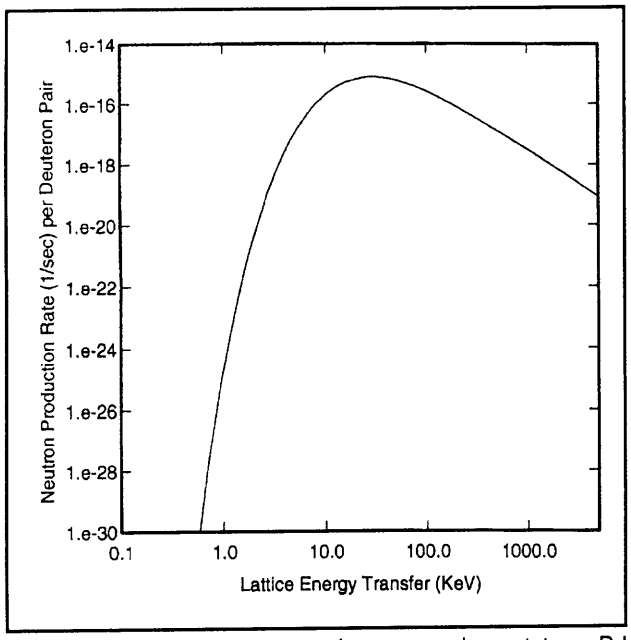

Figure 17. Fusion rate per deuteron pair next to a Pd vacancy.

analog to the equivalent electron matrix elements normally used in Anderson model studies, results in much stronger coupling and very large reaction rate estimates. This model looks very promising; it predicts heat due to neutron transfers from ^{105}Pd to ^{6}Li at 156 KeV lattice energy transfer per reaction to be the dominant heat-producing reaction in Pons-Fleischmann experiments. This work is currently being documented.

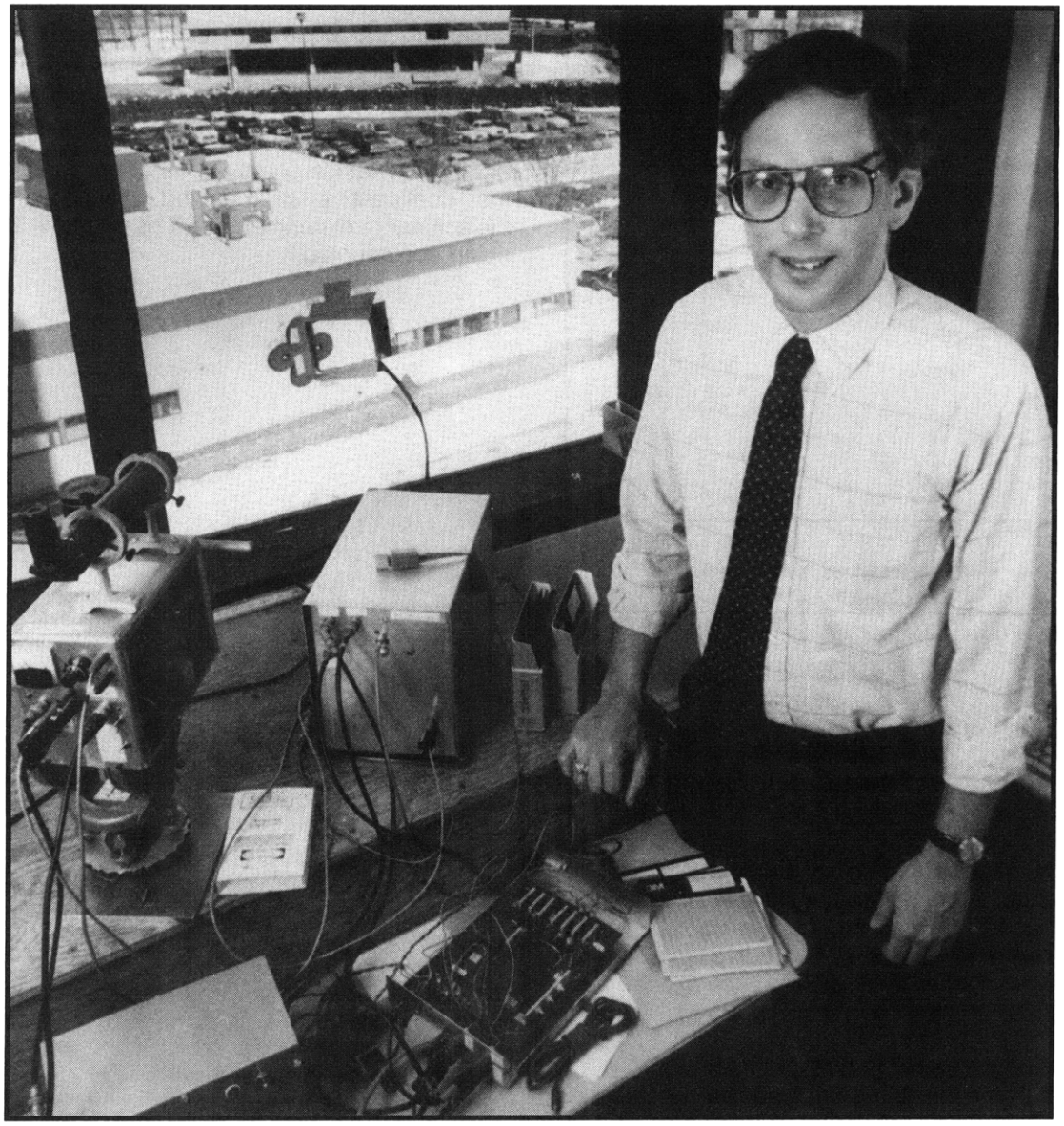

Professor Jeffrey H. Shapiro, Associate Head, Department of Electrical Engineering and Computer Science